AGU PUBLICATIONS

JGR

Journal of Geophysical Research: Earth Surface

RESEARCH ARTICLE
10.1002/2015JF003693

A unified framework for modeling landscape evolution by discrete flows

Eitan Shelef[1,2] and George E. Hilley[1]

[1]Department of Geological and Environmental Sciences, Stanford University, Stanford, California, USA, [2]Now at Department of Geological and Environmental Science, University of Pittsburgh, Pittsburgh, Pennsylvania, USA

Key Points:
- A framework is presented for modeling landscape formation by discrete flows
- Conditions are defined for the formation of hillslopes, channels, and topographic instabilities by discrete flows
- Hillslopes and channels can be viewed as end-members along a continuum controlled by a small number of parameters

Supporting Information:
- Supporting Information S1

Correspondence to:
E. Shelef,
shelef@pitt.edu

Citation:
Shelef, E., and G. E. Hilley (2016), A unified framework for modeling landscape evolution by discrete flows, *J. Geophys. Res. Earth Surf.*, *121*, 816–842, doi:10.1002/2015JF003693.

Received 12 AUG 2015
Accepted 16 MAR 2016
Accepted article online 22 MAR 2016
Published online 3 MAY 2016

Abstract Topographic features such as branched valley networks and undissected convex-up hillslopes are observed in disparate physical environments. In some cases, these features are formed by sediment transport processes that occur discretely in space and time, while in others, by transport processes that are uniformly distributed across the landscape. This paper presents an analytical framework that reconciles the basic attributes of such sediment transport processes with the topographic features that they form and casts those in terms that are likely common to different physical environments. In this framework, temporal changes in surface elevation reflect the frequency with which the landscape is traversed by geophysical flows generated discretely in time and space. This frequency depends on the distance to which flows travel downslope, which depends on the dynamics of individual flows, the lithologic and topographic properties of the underlying substrate, and the coevolution of topography, erosion, and the routing of flows over the topographic surface. To explore this framework, we postulate simple formulations for sediment transport and flow runout distance and demonstrate that the conditions for hillslope and channel network formation can be cast in terms of fundamental parameters such as distance from drainage divide and a friction-like coefficient that describes a flow's resistance to motion. The framework we propose is intentionally general, but the postulated formulas can be substituted with those that aim to describe a specific process and to capture variations in the size distribution of such flow events.

1. Introduction

The morphology of branched valley networks and undissected convex-up hillslopes formed in subaerial environments has been a central thread of investigation of Earth surface studies, which usually associate these features with the flow of water over the Earth's surface and with local processes such as bioturbation, respectively [e.g., *Gilbert*, 1877; *Davis*, 1892; *Gilbert*, 1909; *Horton*, 1945; *Culling*, 1960; *Shreve*, 1966; *Smith and Bretherton*, 1972; *Dunne*, 1980; *Rodríguez-Iturbe et al.*, 1992; *Howard*, 1994; *Dietrich and Perron*, 2006]. However, both branched channel networks and undissected, convex-up hillslopes are also observed in disparate physical environments where occasional mass transport events entrain substrate from landscapes [*McGregor et al.*, 1982; *Pratson and Coakley*, 1996; *Mitchell et al.*, 2002; *Mitchell*, 2005, 2006; *Howard*, 1998; *Treiman*, 2003; *Shinbrot et al.*, 2004; *Dietrich and Perron*, 2006; *Shinbrot*, 2007; *McGuire and Pelletier*, 2013] (Figure 1). For example, occasional density flows dominate entrainment and sediment transport in submarine environments [e.g., *McGregor et al.*, 1982; *Pratson and Coakley*, 1996; *Mitchell et al.*, 2002; *Mitchell*, 2005, 2006], episodic snow avalanches shape the landscape in arctic areas [e.g., *Luckman*, 1977, 1978, 1992; *Shroder et al.*, 1999; *Curry*, 1999], debris flows, landslides, and rock avalanches play a major role in sediment transport over steep mountainous terrain [*Reneau and Dietrich*, 1987; *Montgomery and Buffington*, 1997; *Howard*, 1998; *Stock and Dietrich*, 2003, 2006; *Booth and Roering*, 2011], and localized avalanches probably generate small-scale networks on steep slopes made of snow or loose gravel (Figure 2). In Martian landscapes, several authors have argued that rock avalanches and infrequent granular flows of windblown sand carve gullies commonly observed on steep Martian slopes [*Howard*, 1998; *Treiman*, 2003; *Shinbrot et al.*, 2004; *Shinbrot*, 2007]. Nonfluvial branched channel networks are also formed by granular flow in laboratory experiments at scales <1 m [*Shinbrot et al.*, 2004; *Shinbrot*, 2007].

The fact that different processes give rise to similar forms suggests that common underlying constraints govern the formation of these features across different physical environments, whether they are formed by spatially and temporally discrete or uniform processes. The seminal work of *Smith and Bretherton* [1972]

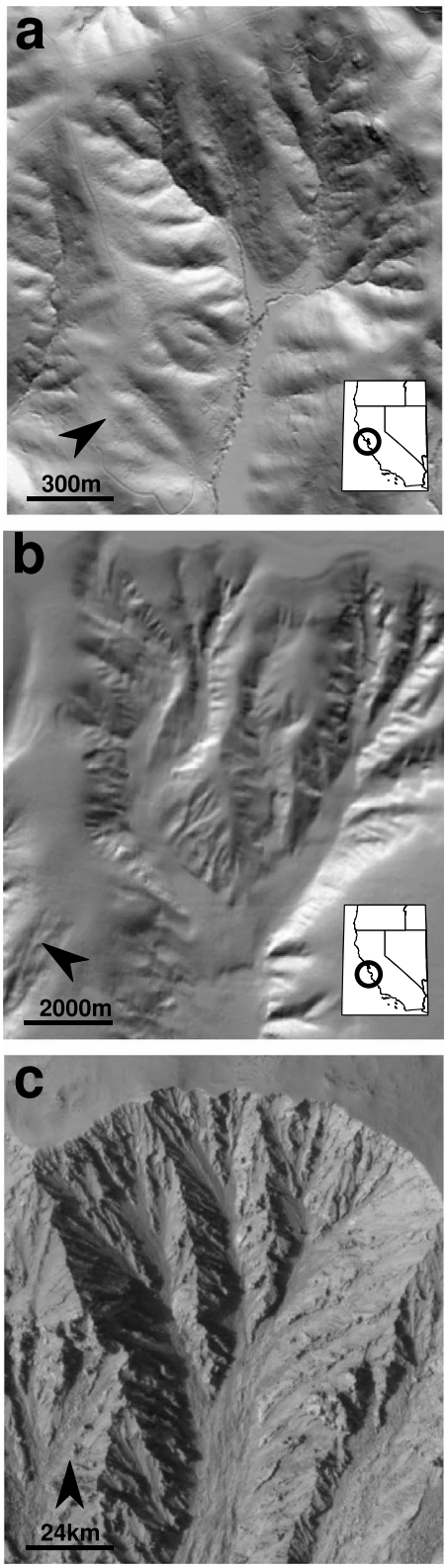

Figure 1. Channel networks in different physical environments: (a) Hillshade image of terrestrial landscape (Tennessee Valley area, California), (b) Hillshade image of a submarine environment off shore of California (Ascension Canyon system, courtesy of Miles Traer). (c) HiRise image of Martian landscape (http://www.uahirise.org/PSP_003939_1420) at approximately 192.9°E, 37.7°S. Black circles over inset maps show terrestrial image locations, and black arrows point northward.

demonstrates that the development of channel networks and undissected hillslopes is dependent on a landscape's resilience to topographic perturbations, which in turn depends on the process that transport sediment in and out of these perturbations. Yet their work casts channel-forming processes in terms of water discharge and uniform rainfall, such that it does not attempt to describe the development of these topographic features in environments dominated by occasional mass transport events. Several studies, however, suggested [*Mitchell*, 2004, 2005; *Stock and Dietrich*, 2006; *Somme et al.*, 2009] and even demonstrated numerically [*Chase*, 1992; *Pratson and Coakley*, 1996; *Crave and Davy*, 2001; *Haff*, 2001] that valley networks may form in environments where flows that are generated discretely in space and/or time (such as debris flows or turbidity currents) converge downslope. *Pratson and Coakley* [1996], for example, used discretely generated submarine flows ("floxels"), induced when prescribed slope failure conditions are attained, to demonstrate that discretely generated submarine flows produce natural-looking bathymetry. In the subaerial environment, *Chase* [1992] demonstrated that the cumulative impact of stochastically generated local precipitation events ("precipitons") can form landscapes that have various degrees of dissection depending on the relations between diffusive, erosive and depositional processes. *Crave and Davy* [2001] extended this approach, and combined a stochastic "preciptons" model with a generalized expression for fluvial sediment transport, where the relative magnitude of erosion and deposition is determined through a single length-scale factor (l_d) [after *Kooi and Beaumont*, 1994, 1996]. A somewhat similar approach was used by *Haff* [2001], who demonstrated that locally generated "waterbots" and "diffusivebots" are capable of producing channels and hillslopes, respectively, and suggested that this approach can be applied to nonfluvial flow types. While these examples span both submarine and subaerial environments, to our knowledge there is currently no framework that casts the conditions for hillslope and channel formation in terms of basic constraints that are common to both discrete and uniformly distributed sediment transport processes.

In this contribution, we present a framework that generalizes the conditions for the formation of different landforms through an explicit dependence between sediment transport rate and the frequency at which discretely generated geophysical flows traverse the landscape. In this framework, the runout distance of flows that are generated discretely in space and/or time (hereafter termed discrete flows) determines the frequency at which upslope-generated flows traverse downslope locations and thus the sediment flux to and from these locations. We postulate simple formulations to demonstrate the effect of runout distance and sediment transport variables on the resulting landscape; however, the framework's structure facilitates substitution of these simple formulations with expressions that are more representative of specific processes. We find that when runout distance is long, a function of low resistance to flow, the temporal averaging of multiple flows may form channelized morphologies equivalent to those produced by overland flow. When runout distance is short (high flow resistance), local sediment transport produces convex-up slope geometries that are identical in functional form to the diffusive idealization of hillslope transport. Additionally, flows that arrest within a landscape may form topographic fluctuations akin to those observed in nature. We thus cast the conditions for landform development in terms of flow resistance and distance from drainage divide, which are likely common to different flow types that shape the various environments where channel networks and undissected hillslopes are observed.

2. Model

2.1. Background

A basis for understanding the conditions that lead to the formation of hillslopes and channel networks is provided by Geomorphic Transport Laws (GTLs) that relate local (e.g., landscape slope) and nonlocal (e.g., upslope catchment area) topographic attributes to mass fluxes and incision rates across landscapes. These rules can be employed with conservation of mass to reveal relationships between land-shaping processes and landscape patterns such as branched valley networks [e.g., *Horton*, 1945; *Howard*, 1971; *Rodríguez-Iturbe et al.*, 1992; *Perron et al.*, 2012; *Willett et al.*, 2014; *Shelef and Hilley*, 2014], the concavity of channel profiles [e.g., *Gilbert*, 1877; *Leopold and Maddock*, 1953; *Smith and Bretherton*, 1972; *Whipple and Tucker*, 1999], and the convexity of hillslopes [e.g., *Davis*, 1892; *Gilbert*, 1909; *Culling*, 1960; *Dunne and Aubry*, 1986; *Roering et al.*, 2001] on this and other planets [*Aharonson et al.*, 2002; *Dietrich and Perron*, 2006; *Black et al.*, 2012]. While the form of a particular GTL depends on the geomorphic transport process considered, all GTLs cast mass transport rate in terms of some measure of the topography and an empirically determined rate constant.

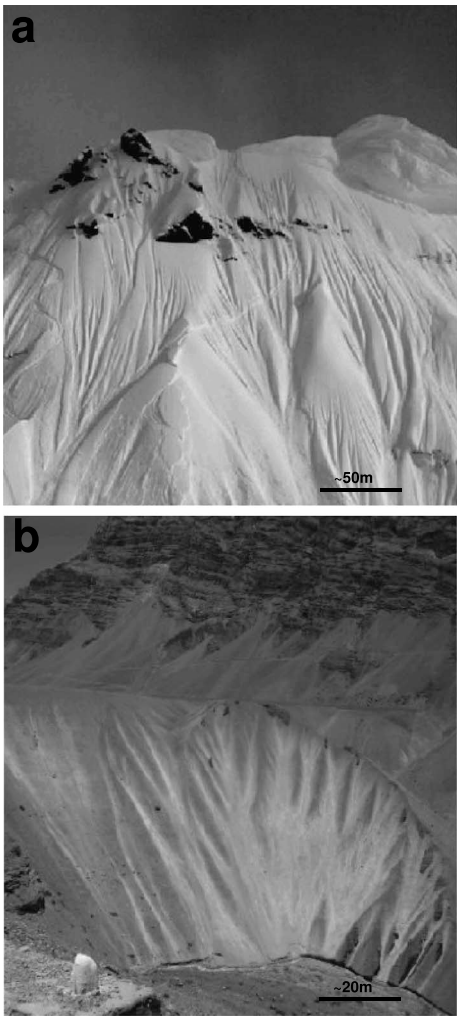

Figure 2. Branched valley networks on steep slopes of (a) dry snow in Alaska (used with permission from Teton Gravity Research [http://www.tetongravity.com/photos]) and (b) loose gravel in the Jammu and Kashmir state at Northern India (courtesy of Dolev Shelef).

Smith and Bretherton [1972] first associated growing topographic instabilities with the initiation and expansion of branched channel and valley networks. They found that these instabilities grow for certain functional forms of GTLs, while other forms damp these instabilities. Prior to this work, it was well known that diffusive-like geomorphic transport processes, whose rates depend solely on the surface slope, evolved toward stable, generally convex or planar landforms. For example, sediment transport rate by processes such as bioturbation or freeze-thaw is often regarded as proportional to the local topographic slope (i.e., diffusive process) [*Davis*, 1892; *Gilbert*, 1909; *Culling*, 1960] as

$$q_{\mathrm{dif}} = -DS\ , \tag{1}$$

where q_{dif} [L^2 't^{-1}] is the sediment transport rate per width (w [L]) due to these diffusive processes, S [] is the local topographic slope, and D [$\mathrm{L}^2\ \mathrm{t}^{-1}$] is a rate constant that scales slope to mass transport rate.

To conserve mass, the spatial divergence of the sediment transport rate per width (q_w, [$\mathrm{L}^2\ \mathrm{t}^{-1}$]) must be accompanied by a change in surface elevation over time:

$$\frac{\mathrm{d}z}{\mathrm{d}t} = u\frac{\rho_r}{\rho_s} - \nabla \cdot q_w\ , \tag{2}$$

where z [L] is elevation, t [t] is time, u [$\mathrm{L}\ \mathrm{t}^{-1}$] is rock uplift rate [e.g., *England and Molnar*, 1990], and ρ_r and ρ_s are the rock and sediment densities [$\mathrm{M}\ \mathrm{L}^{-3}$], respectively. When $q_w = q_{\mathrm{dif}}$, equations (1) and (2) together form

a diffusion equation with a source term (u in this case) that evolves toward a stable geometry when boundary elevations are held constant over time, as the mass transported by hillslope processes removes that provided by uplift or relative base level lowering [e.g., *Culling*, 1960]. In this particular case, landscapes in which a steady state has been achieved (i.e., $dz/dt = 0$) require sediment supply to increase downslope as the source area for sediment increases:

$$q_s = \frac{\rho_r}{\rho_s} uA/w \,, \tag{3}$$

where q_s [$L^2\ t^{-1}$] is the sediment supply rate per unit width that must be transported to maintain steady state. When a diffusive landscape has reached a steady state, we can equate equations (1) and (3), which reveals that slope angles must increase downslope in these landscapes to maintain sediment transport rate equal to sediment supply, resulting in a convex-up form [e.g., *Davis*, 1892; *Gilbert*, 1909]. Under such conditions, the steady state convex-up form is robust to perturbations applied to the surface, as these local zones of low and high slopes on the downslope and upslope sides of the perturbations, respectively, conspire to damp such aberrations over time in a negative feedback [*Smith and Bretherton*, 1972].

In contrast to diffusive transport-limited processes that are dependent only on slope, sediment transport by running water may increase with either slope or water discharge [e.g., *Gilbert*, 1877; *Leopold and Maddock*, 1953; *Smith and Bretherton*, 1972; *Howard and Kerby*, 1983]. In this case, discharge collected upslope may directly affect downslope sediment transport by supplying momentum that may increase transport rates as particles are physically advected across the landscape as suspended load or bed load. Because discharge typically increases with basin area [e.g., *Leopold and Maddock*, 1953], this process is commonly parameterized as [*Flint*, 1973, 1974; *Howard*, 1980; *Willgoose et al.*, 1991a; *Howard*, 1994; *Whipple and Tucker*, 2002]

$$q_n = -kA^{m'} S^{n'} \,, \tag{4}$$

where q_n [$L^2\ t^{-1}$] is the sediment transport rate per unit channel width due to such nonlocal diffusion processes (i.e., a process where the transport rate is dependent on slope, as well as on a nonlocal term). A [L^2] (the nonlocal term) is the upslope drainage area at each point in the landscape, S is the slope, k [$L^{2-2m'}\ t^{-1}$] is an empirically calibrated rate constant, and m' and n' are dimensionless exponents that scale transport to A and S, respectively. Downslope changes in channel width are assumed to have a power law form that is encapsulated in m' and k. Empirical studies suggest that a narrow range of m' and n' values explains the concave-up channel profiles that are ubiquitous in subaerial channel networks [e.g., *Carson and Kirkby*, 1972; *Prosser and Rustomji*, 2000]. When sediment supply is balanced by transport, equation (3) requires that sediment supply increases downslope; however, depending on the values of m' and n', the effect of increasing discharge may produce sediment transport rates in excess of supply for a fixed slope. As the value of m' increases relative to n', convex-up topographic geometries typical of local hillslope processes transition to concave-up convergent geometries [*Kirkby*, 1971, Figure 3]. Interestingly, in cases where such concave profiles form, the the steady state topographic surface is no longer robust to topographic perturbations [*Smith and Bretherton*, 1972]. Instead, the lateral deflection of flow causes localized areas of flow convergence in which transport is accelerated. This causes a positive feedback between transport, surface lowering, and flow convergence [*Smith and Bretherton*, 1972] that may eventually establish a branched network through competition, assimilation, and coevolution of multiple perturbations [e.g., *Willgoose et al.*, 1991b; *Howard*, 1994]. Hence, both profile concavities and plan view branched channel networks appear to be different expressions of processes in which sediment transport rates increase more rapidly downslope than do sediment supply rates for a particular surface slope. The fine-scale extent of these networks is constrained by the magnitude of hillslope-forming processes that damp the growth of these channels [*Loewenherz*, 1991; *Montgomery and Foufoula-Georgiou*, 1993; *Perron et al.*, 2008].

2.2. Analytical Framework for the Formation of Channel Networks and Undissected Hillslopes by Discretely Generated Geophysical Flows

While several mechanisms that rationalize the formation of branched valley networks have been proposed, most invoke flow generated by uniformly distributed rainfall that creates overland flow [e.g., *Horton*, 1945; *Willgoose et al.*, 1991a; *Rodríguez-Iturbe et al.*, 1992; *Howard*, 1994]. As such, the forms of these types of networks have often been associated with specific environments where such conditions prevail. Here we relax the requirement for uniformly distributed, instantaneous rainfall (following *Chase* [1992],

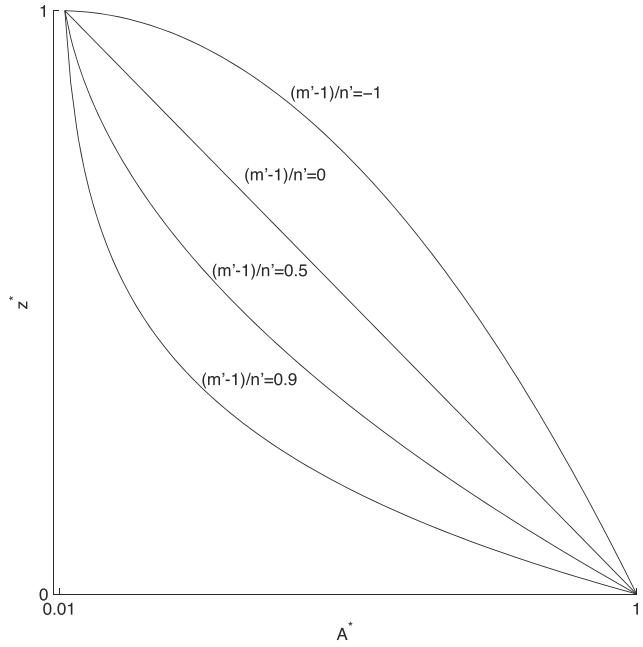

Figure 3. Topographic profiles of various m' and n' values (equation (4), after *Kirkby* [1971]). The y axis is elevation normalized to the maximum elevation ($z^* = z/\max(z)$), and the x axis is drainage area normalized to the maximum drainage area ($A^* = A/\max(A)$). Note that the minimum A^* value is 0.01.

Pratson and Coakley [1996], *Crave and Davy* [2001], and *Haff* [2001]) and propose a general mechanism for the formation of valley networks that accounts for discrete processes in which momentum imparted from upslope locations may affect downslope sediment transport.

We begin by noting that the GTLs described above quantify sediment transport rate by scaling some measure of the topography (i.e., slope, area) by an empirically determined rate constant (e.g., D, k in equations (1), (4)). This approach segregates the topographic attributes (A, S) that scale sediment transport rate and the time scale introduced by the rate constant. Thus, the only mechanism by which transport rates can increase downslope is by a corresponding increase in one of these topographic attributes (e.g., A, S). As a result of the formulation of GTLs, only those processes whose transport rates depend strongly on catchment area can possibly give rise to the positive feedback that is required to induce the growth of perturbations that results in the formation of concave channel networks [i.e., *Smith and Bretherton*, 1972].

The formulation we propose posits that downslope increases in sediment transport rate need not be achieved by increasing discharge but might equally well result from the fact that discrete flows are routed more frequently through convergent, low-lying portions of the landscape. In such a framework, the sediment transport capacity of individual discrete flows may not increase downslope at a magnitude that exceeds sediment supply, yet concave channel networks may still form due to the increased frequency at which flows traverse these convergent, low-lying areas. As such, perturbation growth and channel network development [i.e., *Smith and Bretherton*, 1972] occur when the collection of discrete flows generated throughout the landscape augment the subtle downslope increase in sediment transport capacity of each individual flow such that the collective increase in sediment transport capacity exceeds sediment supply. Undissected hillslopes will form when the downslope collection of flows does not suffice for sediment transport capacity to exceed supply.

We formalize this effect by considering the time-averaged sediment transport rate per width at a point (x, y) as the sum of the sediment transported by all discrete flows that traverse this point within the time span over which this sediment transport rate is averaged. We idealize the sediment transport rate per width for an individual discrete flow, q_p [L^2 t^{-1}], as constant over the duration of the flow (T_d), such that the total volume of sediment per width transported by a given event is determined simply by integrating over its duration. The sediment transport rate at a point due to multiple flows depends on the number of flows that traverse this point within a particular interval of time. This number, in turn, varies with the number of flows that are

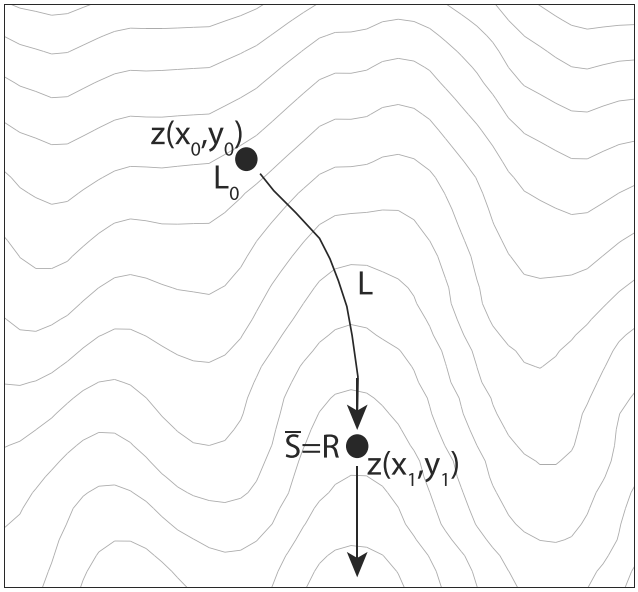

Figure 4. Illustration of a discrete flow generated at (x_0, y_0). Grey contour lines depict the underlying topography (sloping to the lower part of the image). L_0 is a value assigned at $(x, y) = (x_0, y_0)$ to account for local transport processes (see section 2.3.1). L is the distance along the flow route between (x_0, y_0) and (x_1, y_1) (see section 2.3.1). The flow transports sediment, erodes and deposits along its route depending on $L(x, y)$ and $S(x, y)$ (see section 2.3.1), and will arrest where $\bar{S} = \frac{z(x_0,y_0)-z(x,y)}{L}$ equals the flow resistance coefficient (R, see section 2.3.3). If $\bar{S} = R$ occurs at (x_1, y_1), the flow will arrest such that the binary function $f(x_0, y_0, x, y, \xi)$ equals zero everywhere downslope of this point (i.e., equation (5)) and one upslope of it.

generated per area per time (hereafter referred to as the generation frequency, F [L^{-2} t^{-1}]). Likewise, the routing of these flows to the point (x, y) through the upslope topography determines how frequently these discretely generated flows will traverse the point (x, y) and thus the sediment transport rate at this point. For simplicity, we assume that all flows have the same duration (T_d), so that the sediment transport rate per width due to all discrete flows (q_a [L^2 t^{-1}]) is

$$q_a(x, y, t) = \int_{-\infty}^{\infty} \int_{-\infty}^{\infty} \int_{0}^{T_d} F(x_0, y_0, S, A) q_p(x_0, y_0, x, y, \xi) f(x, y, x_0, y_0, \xi) \mathrm{d}t \mathrm{d}x_0 \mathrm{d}y_0 \ , \quad (5)$$

where x_0 and y_0 are the locations at which flows are generated (Figure 4), $f(x_0, y_0, x, y, \xi)$ is a dimensionless binary function that describes routing of flows across the surface and assumes a value of one if a flow generated at (x_0, y_0) traverses the point (x, y) and a value of zero if it does not. $\xi(x, y, t)$ is a state variable that describes the characteristics of a flow (e.g., mass, density, viscosity, and grain size distribution) at the point (x, y) and time t, which acknowledges that these characteristics may change with space (x, y) and time (t) due to the detailed dynamics of the flow and its interaction with the underlying substrate. As such, $\xi(x, y, t)$ can describe flows of different magnitude and rheology. ξ might also empirically incorporate the impact of interactions between temporally overlapping flows that traverse the same point in a landscape (e.g., rainfall-induced parcels of water that coalesce downslope and increase discharge), although we do not formalize or explore its effect in this study. For the sake of generality, we allow the flow generation frequency ($F(x_0, y_0, S, A)$) to vary over the surface, as well as with topographic characteristics at (x_0, y_0) (encapsulated in S and A). Note that this formulation allows for a flow, such as fluvial flow, to traverse a landscape location ($f(x, y, x_0, y_0, \xi) = 1$) while carrying no sediments ($q_p(x_0, y_0, x, y, \xi) = 0$).

In this framework, the frequency at which discrete flows traverse different landscape localities depends explicitly on the frequency at which they are generated ($F(x_0, y_0, S, A)$) and the way in which they are routed through the upslope topography ($f(x_0, y_0, x, y, \xi)$). The dependence of f on ξ accounts for the effect of flow-substrate interactions on the distance (L) to which flows may run downslope:

$$L = \zeta(x_0, y_0, x, y, \xi) \ , \quad (6)$$

where ζ is a function parameterized in a way that captures the dependence of flow runout distance on flow properties as well as on upslope and local topography.

The combination of $F(x_0, y_0, S, A)$ and $f(x_0, y_0, x, y, \xi)$ explicitly links the topography of the landscape to the time scale of sediment transport, which disentangles the time and space scales that are subsumed into the spatially unvarying rate constant typically used in GTLs. Such an approach provides a rational means of modeling natural flows whose frequency of traversing points within a landscape may depend on the flow dynamics as well as on local topographic, lithologic, and climatic attributes.

2.3. Specific Model Formulation

2.3.1. Postulated GTL

It is possible to substitute q_p (equation (5)) with a particular GTL that describes a process of interest in the general framework described by equation (5). For illustration, we construct a simple GTL that allows discrete flows to erode and deposit throughout their route. In this GTL q_p is a function of the magnitude of the local topographic slope, $S(x, y)$ [], and the runout distance of the flow, $L(x, y, x_0, y_0)$ [L] from the point where it is generated (x_0, y_0) to the point of interest (x, y) (Figure 4):

$$ {}^{s}q_p(x, y) = -k_{df}(\xi, x, y)[S(x, y)]^{n(\xi)}[L(x_0, y_0, x, y)]^{m(\xi)} \tag{7} $$

${}^{s}q_p$ [L^2 t^{-1}] is the sediment transport rate per width for this particular formulation, $m(\xi)$ and $n(\xi)$ are dimensionless exponents that depend on the process of sediment transport (captured in the local flow characteristics $\xi(x, y, t)$) and allow nonlinearity in the relations between sediment transport and S and L [e.g., *Gilbert*, 1877; *Kirkby*, 1971; *Willgoose et al.*, 1991a]. The inclusion of S and L conceptually captures the impact of gravity and of momentum imparted from upslope areas of the flow, respectively, on ${}^{s}q_p$ and allows for erosion and deposition along the flow's route. The empirical factor k_{df} [$L^{2-m}t^{-1}$] scales sediment transport rate to the local topographic characteristics by subsuming the effect of flow dynamics on sediment transport into a function that varies with flow location and state. Substituting equations (7) into equation (5) gives the sediment transport rate per width due to all flows for this particular formulation (${}^{s}q_a$ [L^2t^{-1}]):

$$ {}^{s}q_a(x, y) = -\int_{-\infty}^{\infty}\int_{-\infty}^{\infty}\int_{0}^{T_d} F(x_0, y_0, S, A)k_{df}(\xi, x, y)[L(x_0, y_0, x, y)]^m[S(x, y)]^n f(x, y, x_0, y_0, \xi)\mathrm{d}t\ \mathrm{d}x_0\ \mathrm{d}y_0 \tag{8} $$

Finally, we substitute q_w with ${}^{s}q_a$ in equation (2) to describe changes in surface elevation in response to sediment transport by discrete flows.

In some cases sediment transport may occur locally without a flow running out over the landscape, such as with tree throw or other bioturbative processes [e.g., *Roering et al.*, 1999, 2001]. To account for these cases we introduce $L_0(x_0, y_0)$, so that when $(x, y) = (x_0, y_0)$, the runout length of a flow is set to L_0 and $f(x_0, y_0, x, y, \xi)$ is set to one, such that the value of L_0 determines the magnitude of these local processes.

2.3.2. Detachment-Limited Conditions

While the proposed framework is cast in terms of sediment transport rate and focuses on transport-limited conditions [e.g., *Howard*, 1994; *Whipple and Tucker*, 2002] that describe both local and nonlocal diffusive processes, a slight modification facilitates a description of detachment-limited conditions [e.g., *Howard*, 1994; *Whipple and Tucker*, 1999]. These conditions, where surface lowering is limited by the flow's ability to detach material from the substrate rather than by transport capacity, are described by modifying equation (5) so that its left-hand side (LHS) equals erosion rate ($\dot{E}$) [L t^{-1}], and q_p is substituted by the erosion rate produced by a flow (q_{pe} [L t^{-1}]).

$$ \dot{E}(x, y, t) = \int_{-\infty}^{\infty}\int_{-\infty}^{\infty}\int_{0}^{T_d} F(x_0, y_0, S, A)q_{pe}(x_0, y_0, x, y, \xi)f(x, y, x_0, y_0, \xi)\mathrm{d}t\mathrm{d}x_0\mathrm{d}y_0 \tag{9} $$

Substitution of $\dot{E}$ with $\nabla \cdot q_w$ in equation (2) describes changes in surface elevation in response to detachment-limited erosion caused by discrete flows:

$$ \frac{\mathrm{d}z}{\mathrm{d}t} = u\frac{\rho_r}{\rho_s} - \dot{E}(x, y, t) \tag{10} $$

2.3.3. Postulated Energy-Based Control on Runout Distance

To examine the topographic impact of flows whose runout (L) is constrained by both topography and flow properties (i.e., equation (6)), we use a simple energy balance in which the runout distance of a flow (and thus the value of $f(x_0, y_0, x, y, \xi)$) is determined by a balance between its initial potential energy and the work done by a resisting force throughout its route [e.g., *Heim*, 1932; *Hsu*, 1975; *Straub*, 1996; *Iverson*, 1997]. For small slope angles:

$$Mg\Delta H = MgR\Delta L\ , \tag{11}$$

where M [M] is flow mass, g [L t^{-2}] is gravitational acceleration, ΔH [L] is elevation difference along flow route, R [] is a resistance coefficient, and ΔL [L] is horizontal runout distance along the route of the flow. Note that $R = \Delta H/\Delta L$ when mass is neither gained or lost along a given flow path, which represents a critical mean slope, $\overline{S}$, that is required to maintain flow motion (Figure 4).

We acknowledge the apparent discrepancy between the changing mass of an entraining and/or depositing flow (e.g., equation (7)) and the assumption of constant mass embedded in equation (11). However, as pointed out by *Iverson* [1997], changes in flow mass are tied to complex momentum exchanges between the flow, the bed, and the banks, such that a universal energy budget that captures the impact of these external forcings on the flow's mass exchange is difficult to simulate. We thus choose this simple energy balance (following *Heim* [1932], *Hsu* [1975], *Straub* [1996], and *Iverson* [1997]) and demonstrate that even this exceedingly simple description can produce discrete flows that give rise to the formation of landforms such as branched valley networks and undissected hillslopes. We reiterate that the purpose of equation (11) is to demonstrate the impact of a constrained flow's runout distance on the topography, regardless of a specific process and that equation (6) facilitates substitution of this simple constraint with those that are formulated specifically for processes of interest [e.g., *Scheidegger*, 1973].

2.4. Nondimensionalization

To better understand how the terms in equations (2), (5), and (8) control the scaling and behavior of the proposed framework, we first nondimensionalize the rate of change of surface elevation at each point along the landscape (equation (2)). To do so, we define characteristic length (l_c) and time (t_c) scales, and use them to define the dimensionless groups: $t^* = t/t_c, z^* = z/l_c, x^* = x/l_c, y^* = y/l_c, \rho^* = \rho_r/\rho_s, u^* = ut_c/l_c, q_w^* = q_w t_c/l_c^2$, and $\nabla^* = l_c\nabla$. This gives:

$$\frac{\mathrm{d}z^*}{\mathrm{d}t^*} = u^*\rho^* - \nabla^* \cdot q_w^* \tag{12}$$

To examine the case where the sediment transport rate per unit width, q_a, is expressed by equation (5), we substitute equation (5) into equation (2) and introduce the dimensionless groups: $T_d^* = T_d/t_c$, $A^* = A/l_c^2$, $x_0^* = x_0/l_c$, $y_0^* = y_0/l_c$, $q_p^* = q_p t_c/l_c^2$, $F^* = Fl_c^2 t$. With these length and time scales, equation (5) can be written in its nondimensional form as

$$\frac{\mathrm{d}z^*}{\mathrm{d}t^*} = u^*\rho^* - \nabla^* \cdot \int_{-\infty}^{\infty}\int_{-\infty}^{\infty}\int_{0}^{T_d^*} F^*\left(x_0^*, y_0^*, S, A^*\right) q_p^*\left(x_0^*, y_0^*, x^*, y^*\right) f\left(x^*, y^*, x_0^*, y_0^*, \xi\right) \mathrm{d}t^*\mathrm{d}x_0^*\mathrm{d}y_0^* \tag{13}$$

Finally, for the case where q_p is described by the postulated GTL (equation (7)), we let, for convenience, F and k_{df} be constant in space and time, and define $K = FT_d k_{df}$. We further define $L^* = L/l_c$, and let $l_c = (u_0/K)^{1/(m+1)}$, and $t_c = (u_0^m K)^{-1/(m+1)}$, where u_0 is a reference uplift rate. When $\rho_r = \rho_s$ this results in

$$\begin{aligned}\frac{\mathrm{d}z^*}{\mathrm{d}t^*} &= 1 - \nabla^* \cdot q_a^* \\ &= 1 + \nabla^* \cdot \left[S\left(x^*, y^*\right)\right]^n \int_{-\infty}^{\infty}\int_{-\infty}^{\infty} \left[L^*\left(x_0^*, y_0^*, x^*, y^*\right)\right]^m f\left(x^*, y^*, x_0^*, y_0^*, \xi\right) \mathrm{d}x_0^*\mathrm{d}y_0^*\ ,\end{aligned} \tag{14}$$

such that the change in dimensionless surface elevation is described by the dimensionless length and location quantities ($L^*, x_0^*, y_0^*, x^*, y^*, \nabla^*$), and by the surface slope (S []).

In the one-dimensional case, where $\mathrm{d}y^* = w^* = w/l_c$, this results in

$$\frac{\mathrm{d}z^*}{\mathrm{d}t^*} = 1 + w^*\frac{d}{dx^*}\left[S\left(x^*, y^*\right)\right]^n \int_{-\infty}^{\infty}\left[L^*\left(x_0^*, y_0^*, x^*, y^*\right)\right]^m f\left(x^*, y^*, x_0^*, y_0^*, \xi\right) \mathrm{d}x_0^* \tag{15}$$

2.5. Numerical Implementation

We use a node-centered finite volume numerical scheme to solve a discrete version of equation (14) over a rectangular grid $z^*_{i,j}(x_i, y_j)$ with grid spacings $\Delta x^* = \Delta x/l_c$ and $\Delta y^* = \Delta y/l_c$, such that

$$\begin{aligned} z^*_{i,j}(x_i, y_j) &= z^*(x_i, y_j) \\ x^*_i &= i\Delta x^* \\ y^*_j &= j\Delta y^* \\ i &= 0, 1, 2 \ldots N_x - 1 \\ j &= 0, 1, 2 \ldots N_y - 1 \end{aligned} \tag{16}$$

where N_x and N_y are the grid dimensions in the x and y directions. Equation (14) can thus be written in a discrete form:

$$\frac{\Delta z^*}{\Delta t^*} = 1 - \nabla^*_d \cdot q^*_d \tag{17}$$

where q^*_d and ∇^*_d are the discrete forms of the dimensionless sediment transport rate and divergence operator, respectively.

In equation (17), q^*_d is calculated in the downslope direction determined by a D_4 routing rule in which flows are routed to one of the surrounding four orthogonal grid nodes, (x^*_n, y^*_m), located in the direction of steepest descent. D_4 was chosen to avoid the dimensional inconsistency associated with flow routing through cell corners and for algorithmic simplicity and efficiency [*Costa-Cabral and Burges*, 1994; *Moore and Grayson*, 1991; *Chirico et al.*, 2005; *Shelef and Hilley*, 2013]. Thus, x_n can equal x^*_{i-1}, x^*_i, or x^*_{i+1}, and y^*_m can equal y^*_{j-1}, y^*_j, or y^*_{i+j}. (x^*_{in}, y^*_{jm}) is the location of the cell boundary midway between (x^*_i, y^*_j) and the node of steepest descent, so that x^*_{in} can equal $x^*_{i\pm1/2} = x^*_i \pm \Delta x/2$ or x^*_i, and y^*_{jm} can equal $y^*_{j\pm1/2} = y^*_j \pm \Delta y/2$ or y^*_j. The dimensionless sediment transport rate at the cell boundary in the direction of steepest descent is thus

$$\begin{aligned} q^*_d\left(x^*_{in}, y^*_{jm}\right) = \Delta x^* \Delta y^* \frac{W^*}{\Delta^*_e} \left|S\left(x^*_{in}, y^*_{jm}\right)\right|^n \sum_{i0=0}^{N_x-1} \sum_{j0=0}^{N_y-1} \left[L^*\left(x^*_{i0}, y^*_{i0}, x^*_{in}, y^*_{jm}\right)\right]^m \\ f\left(x^*_{i0}, y^*_{i0}, x^*_{in}, y^*_{jm}\right) \end{aligned} \tag{18}$$

where $L^*(x^*_{i0}, y^*_{i0}, x^*_{in}, y^*_{jm})$ is the nondimensional flow runout length in the downslope direction to the point (x^*_{in}, y^*_{jm}). $S(x^*_{in}, y^*_{jm}) = \frac{z^*(x^*_n, y^*_m) - z^*(x^*_i, y^*_j)}{\Delta^*_e}$, where $\Delta_e = \Delta x = \Delta y$ and $\Delta^*_e = \Delta_e/l_c$. $(x^*_{i0},\ y^*_{j0})$ is the location of flow generation where i_0, j_0 are the indices of the node where flow is generated so that $x^*_{i0} = i_0\Delta x^*$ and $y^*_{j0} = j_0\Delta y^*$. The factor $\frac{W^*}{\Delta^*_e}$ accounts for the finite flow width (W, where $W^* = W/l_c$) [i.e., *Howard*, 1994], which is prescribed here as a constant whose value does not exceed the dimensionless grid spacing Δ^*_e [e.g., *Perron et al.*, 2008]. The discrete divergence of q^*_d equals

$$\nabla^*_d \cdot q^*_d\left(x^*_i, y^*_j\right) = \frac{q^*_d\left(x^*_{i+1/2}, y^*_j\right) - q^*_d\left(x^*_{i-1/2}, y^*_j\right)}{\Delta x^*} + \frac{q^*_d\left(x^*_i, y^*_{j+1/2}\right) - q^*_d\left(x^*_i, y^*_{j-1/2}\right)}{\Delta y^*} \tag{19}$$

where the sign of q^*_d is set to positive when flows are directed to the south and west and to negative when they are directed to the north and east, where x^* and y^* increase to the east and to the north, respectively.

To capture the stochastic generation of discrete flows and address numerical instabilities that occur when $R = S$ (section 3.2) we prescribed stochastic flow generation over the model domain. To do so, we noted that the mean number of flows ($\bar{n_f}$) generated within a prescribed nondimensional model element area ($\Delta x^* \times \Delta y^* = \Delta^{*2}_e$) and time step ($\delta t^*$) must be equal to one. In these stochastic simulations, flows are generated at this mean frequency using the following procedure. First, the nondimensional cell dimensions ($\Delta x^*,\ \Delta y^*$) are determined at the beginning of the simulation and from these values δt^* is calculated as $(\Delta x^* \times \Delta y^*)^{-1}$. Second, flows are generated during each nondimensional model time increment (δt^*) by drawing a random number (r_n) in the interval [0,1] for each model cell. The number of flows is assigned as follows to achieve a mean frequency of one flow per cell during the time increment δt^*: zero flows when $0 \le r_n < 0.25$, one flow when $0.25 \le r_n < 0.75$, and two flows when $0.75 \le r_n < 1$.

When the number of flows generated at (x^*_{i0}, y^*_{j0}) is >0 we calculate the contribution of these flows to the dimensionless sediment transport (q^*_d) through both local and nonlocal processes. Sediment transport

through local diffusion is simulated by setting $L^* = L_0^*$, $f(x_{i0}^*, y_{j0}^*, x_i^*, y_j^*, \xi) = 1$ at the downslope boundary of the point (x_{i0}^*, y_{j0}^*). Transport by nonlocal diffusion is calculated from the runout distance of flows, where flows are allowed to run downslope as long as $\bar{S}$ along their flow route is greater than R. This constraint also prevents flows from initiating when $S(x_{in}^*, y_{jm}^*) < R$. Once flows run downslope, L^* is calculated at each boundary between nodes for each generated flow in the grid. These L^* values are then used to calculate the nondimensional sediment transport rate ($q_d^*(x_{in}^*, y_{jm}^*)$) due to the cumulative impact of all flows (equation (18)), such that the mass of a flow can change as it runs downslope. These transport rates are then used to determine the elevation at the end of the time increment δt^* using forward Euler integration with Von Neumann stability criteria. This process is repeated for each time increment δt^*.

Boundary conditions are specified as follows: (1) A no flux boundary through which water and sediments are prevented from passing is set at $y^* = 0$. (2) A constant elevation boundary through which water and sediment could pass is specified at $y^* = L_{sy}^*$, where L_{sy}^* is the length of the model domain in the y dimension. (3) A periodic boundary is prescribed at $x^* = 0$, $x^* = L_{sx}^*$ (where L_{sx}^* is the length of the model domain in the x dimension) such that the inflow of sediment from one side of the model was set equal to the outflow of this mass on the other side. The 1-D simulations have similar boundary conditions except that the $x^* = 0$, $x^* = L_{sx}^*$ boundaries are prescribed as no flux boundaries.

To ensure equivalence between the initial conditions of all simulations, we prescribed initial conditions as follows. First, we calculated an inclined planar topography whose slope equals R and is inclined toward the constant elevation boundary at $y^* = L_{sy}^*$. Next, we applied uniform random noise to the surface to facilitate lateral flow convergence. The magnitude of this noise was scaled by the magnitude of the slope of the initial surface such that the mean local slope at individual nodes was $10 \times R$ (this value was determined by experiments that revealed the approximate noise level required to produce significant flow convergence). For the case of $R = 0$, we repeated the above procedure with a small (1×10^{-6}) initial slope that can trigger flow runout and sediment transport.

To explore topographic patterns and fluctuations of the simulated landscapes, each simulation was run until it attained a time-averaged steady state relief, where temporal fluctuations in the mean relief have a similar magnitude and are centered around the same temporal mean. We then generated 200 sequential simulated topographies produced every δt^* and calculated the values of the 10th, 50th, and 90th percentiles ($p_{c10}, p_{c50}, p_{c90}$, respectively) of dimensionless surface elevation and slope over these 200 dimensionless time steps. We calculated channel concavity (i.e., θ, the negative of the slope regressed from the logarithmic S versus A relations [e.g., *Flint*, 1974; *Howard and Kerby*, 1983]) from S and A^* computed for each node after topographic pits were filled.

3. Results

3.1. Reconciliation of Local and Nonlocal Diffusive Sediment Transport as Processes With Different Flow Runout Distance

3.1.1. Local Diffusive Sediment Transport

We first examine the case in which the resistance coefficient is everywhere larger than the local slope ($R > S$). In this case, generated flows do not run out such that $L > 0$ and $f(x_0, y_0, x, y, \xi) = 1$ only at the point $(x, y) = (x_0, y_0)$ where $L = L_0$ to account for local sediment transport. For simplicity, we assume that the frequency of flow generation is uniform across the landscape, such that $F(x_0, y_0, S, A) = F_0$, and transform equation (8) into radial coordinates:

$$ {}^{s}q_a(r_0, \theta_0, t) = -F_0 k_{df} T [S(r, \theta)]^n \int_{-\pi}^{\pi} \int_0^{L_0} r L_0^m f(r)\, \mathrm{d}r\, \mathrm{d}\theta \tag{20} $$

where r ranges from zero to L_0, $f(r) = f(x_0, y_0, x, y, \xi)$, and (r_0, θ_0) is the location of x_0, y_0. Integrating equation (20) gives

$$ {}^{s}q_a(r_0, \theta_0) = -F_0 k_{df} T \pi L_0^{m+2} [S(r, \theta)]^n = -D' [S(r, \theta)]^n , \tag{21} $$

where $D' = \pi F_0 k_{df} T L_0^{m+2}$ [$\mathrm{L}^2\ \mathrm{t}^{-1}$]. Thus, when flows do not run out, they produce forms equivalent to those previously idealized as arising from local diffusive transport (i.e., equation (1)), which results in the formation of convex-up undissected hillslopes.

To numerically explore this case, where $R > S$ over the entire landscape, we prescribed an R value (Table S1) that is much larger than the maximal slope calculated for a 1-D convex-up surface (S_{vx}) of length L_{sy}^* ($R >> S_{vx}(L_{sy}^*)$,

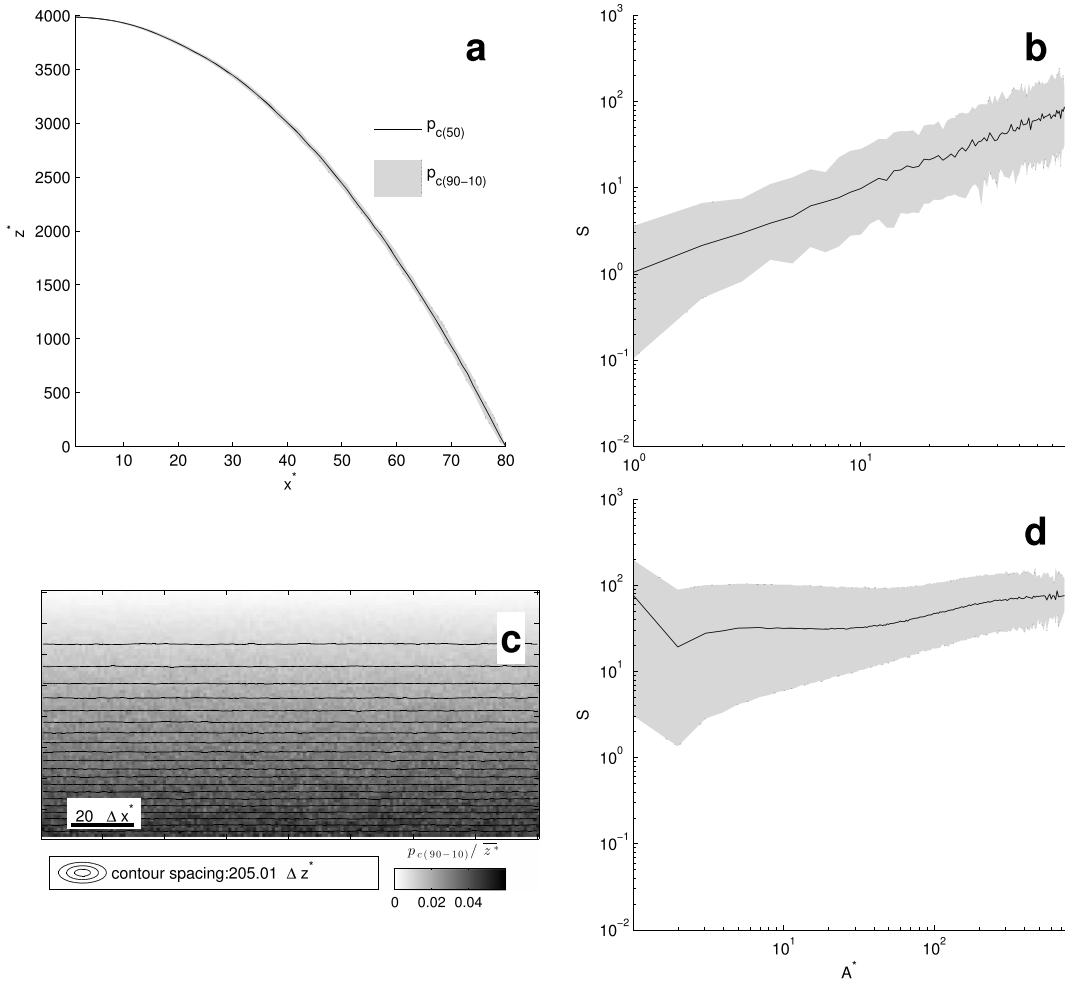

Figure 5. Topography of convex-up surface formed by local diffusion processes (i.e., section 3.1.1). Here $R >> |S_{vx}(L^*_{sy})|$, where $S_{vx}(L^*_{sy})$ is the slope of steady state convex-up 1-D landscape at a distance of model length from the divide. (a) Topography of a 1-D simulated landscape strip. The elevation at each node is the median elevation of 200 consequent simulated topographies generated every δt^* after the simulated surface attained approximately constant relief. The values of $p_{c(50)}$ and $p_{c(90-10)}$ reflect the median elevation of the 200 simulated topographies, as well as the elevation values bounded between the 10th and 90th percentiles of these simulated topographies, respectively. (b) Slope-area relations for the area shown in Figure 5a. (c) Topography of simulated 2-D topography. Contours portray the median elevation for each node over 200 consequent simulated topographies generated every δt^* after the simulated surface attained approximately constant relief. The regional slope is oriented from the top to the bottom of the figure. Colors mark the normalized magnitude of elevation fluctuations ($p_{c(90-10)}/\bar{z}^*$) over this time period for each node, where $\bar{z}^*$ is the mean p_{c50} of dimensionless elevation for these 200 simulated topographies over the entire simulated landscape. (d) Slope-area relations for the 2-D landscape shown in Figure 5c. The greyed zone indicates the 10th and 90th slope percentiles.

Table S1 in the supporting information). The 1-D simulation (Figures 5a and 5b) produces a convex-up topography with a concavity of $\bar{\theta} = -1$. The 2-D simulation (Figures 5c and 5d) produces an overall smooth convex-up topography. In contrast to the 1-D simulation, the concavity of the 2-D simulation is $\bar{\theta} = -0.23$ where low A^* values are associated with overall higher slope values than those of the 1-D simulation.

3.1.2. Nonlocal Diffusive Sediment Transport

The second end-member scenario we consider is the case in which $R < S$ everywhere, so that R does not constrain the flow's runout distance. We assume that flows are generated uniformly across the surface ($F(x_0, y_0, S, A) = F_0$) such that:

$$ {}^{s}q_a(x,y,t) = -F_0 T k_{df} S(x,y)^n \int_{-\infty}^{\infty}\int_{-\infty}^{\infty} [L(x,y,x_0,y_0)]^m f(x_0,y_0,x,y)\mathrm{d}x_0\mathrm{d}y_0 \quad (22) $$

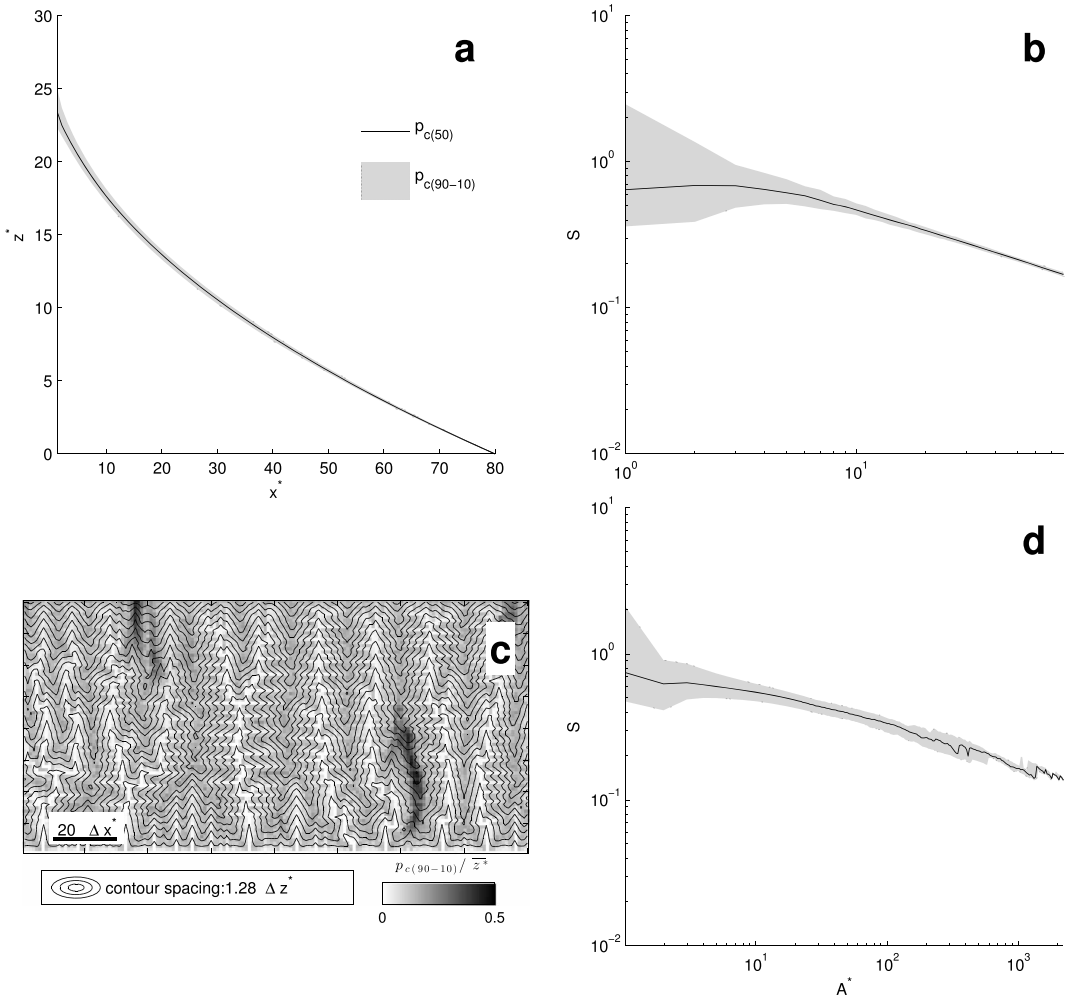

Figure 6. Topography of concave-up surface formed by nonlocal diffusion processes (i.e., section 3.1.2) simulated with $R = 0$. (a) Topography of a 1-D simulated landscape strip. The elevation at each node is the median elevation of 200 consequent simulated topographies generated every δt^* after the simulated surface attained approximately constant relief. The values of $p_{c(50)}$ and $p_{c(90-10)}$ reflect the median elevation of the 200 simulated topographies, as well as the elevation values bounded between the 10th and 90th percentiles of these simulated topographies, respectively. (b) Slope-area relations for the area shown in Figure 6a. (c) Topography of simulated 2-D topography. Contours portray the median elevation for each node over 200 consequent simulated topographies generated every δt^* after the simulated surface attained approximately constant relief. The regional slope is oriented from the top to the bottom of the figure. Colors mark the normalized magnitude of elevation fluctuations ($p_{c(90-10)}/\bar{z}^*$) over this time period for each node, where $\bar{z}^*$ is the mean p_{c50} of dimensionless elevation for these 200 simulated topographies over the entire simulated landscape. (d) Slope-area relations for the 2-D landscape shown in Figure 6c. The greyed zone indicates the 10th and 90th slope percentiles. Note the downslope reduction of the greyed zone bounded between p_{c90} and p_{c10} in Figure 6a, and the relatively low values of $p_{c(90-10)}/\bar{z}^*$ within channels in Figure 6c.

The double integral on the right-hand side (RHS) of equation (22) integrates transport over the area that drains to a particular point (x, y). By transforming Cartesian coordinates into a coordinate system in which catchment area is related to flow length as a power function (a typical relation for various environments and processes [*Hack*, 1957; *Mitchell*, 2005; *Stepinski et al.*, 2002])

$$A = k_a L^h \,, \tag{23}$$

and noting that $f(x_0, y_0, x, y) = 1$ everywhere within a basin in this new coordinate system, equation (22) can be written as

$${}^s q_a(L,t) = -F_0 T k_{df} S(L)^n \int_A L^m \mathrm{d}A \tag{24}$$

By using equation (23) to cast equation (24) in terms of A,

$$ {}^{s}q_a(A,t) = -F_0 T k_{df} S(A)^n \int_A \left(\frac{A}{k_a}\right)^{m/h} \mathrm{d}A \tag{25} $$

Finally, equation (25) and its limits can be cast in terms of L by noting that

$$ \mathrm{d}A = h k_a L^{h-1} \mathrm{d}L \tag{26} $$

such that

$$ {}^{s}q_a(L,t) = -F_0 T k_{df} S(L)^n \int_0^L L^{m+h-1} h k_a \mathrm{d}L \tag{27} $$

yielding ${}^{s}q_a(L,t) = -\frac{F_0 T k_{df} k_a h S(L)^n}{m+h} L^{m+h}$, when $m+h \neq 0$, and ${}^{s}q_a(L,t) = -F_0 T k_{df} k_a h S(L)^n \ln(L)$, when $m+h=0$. Substituting L with A using Hack's law (equation (23)) gives

$$ {}^{s}q_a(a,t) = -\frac{F T k_{df} h k_a^{-m/h}}{m+h} A'^{m/h+1} S^n = -k_A A'^{M'} S^n \tag{28} $$

where $M' = m/h + 1$ (when $m+h=0$, ${}^{s}q_a(a,t) = -F T k_{df} k_a^{-m} \ln[\frac{A'}{k_a}] S^n$). This form is equivalent to that of equation (4), indicating that this specific end-member condition allows the proposed framework to subsume nonlocal diffusive sediment transport akin to that of fluvial processes.

To simulate the scenario where $R < S$ everywhere, we prescribed $R = 0$ such that the runout distance of the flow is not constrained by flow resistance. The 1-D simulation (Figures 6a and 6b) produces a concave-up topography of average concavity $\bar{\theta} = 0.42$. The degree of elevation fluctuations decreases gradually downslope toward the model boundary at L_{sy}. The 2-D simulation (Figures 6c and 6d) produces branched channel networks where topographic fluctuations on drainage divides are higher than within channels. Relatively high topographic fluctuations at the top left and bottom right portions of the landscape are associated with lateral divide migration. The average concavity of the 2-D simulations is about half than that of the 1-D landscape ($\bar{\theta} = 0.25$).

3.2. The Impact of Flow Runout on Topographic Fluctuations

The end-member conditions examined in section 3.1 occur when the conditions $S > R$ or $S < R$, which favor concave and convex topography, respectively, hold over the entire landscape. However, this may not always be the case due to changes in S in response to uplift and sediment transport. We next use equations (11) and (15) to explore how the coevolution of topography and transport may form conditions in which the end-member scenarios examined in section 3.1 are limited to only a fraction of a landscape. To do this, we examine how uplift and sediment transport determine the spatial extent where these end-member conditions hold.

First, we consider the extent of convex-up forms in the landscape. The nondimensional distance from the divide (${}^{d}L_R^*$) over which this condition applies can be evaluated in the context of equation (15) by assigning $S({}^{d}L_R^*) = R$, rearranging and integrating (for $m \neq 1$), so that

$$ {}^{d}L_R^* = w^* \frac{L_0^{*m+1}}{m+1} R^n \tag{29} $$

Thus, portions of the landscape located at $x^* < {}^{d}L_R^*$ will be expected to host convex-up geometries typical of local processes (i.e., equation (1)) and portions where $x^* > {}^{d}L_R^*$ may enable generation of flows that run out.

The conditions that favor concave-up topography are those where $S > R$ such that flows run out downslope. The nondimensional distance from the divide (${}^{a}L_R^*$) over which this condition operates can be evaluated in the context of equation (15) by assigning $S({}^{a}L_R^*) = R$, ${}^{a}L_R = L^*$, $m \neq 1$, rearranging and integrating, so that

$$ {}^{a}L_R^* = \left(\frac{m+1}{w^* R^n}\right)^{1/m} \tag{30} $$

In these cases, flows generated at locations upslope of ${}^{a}L_R^*$ will run downslope such that portions of the landscape located at $x^* < {}^{a}L_R^*$ will be expected to host concave-up geometries. Portions where $x^* > {}^{a}L_R^*$ may be

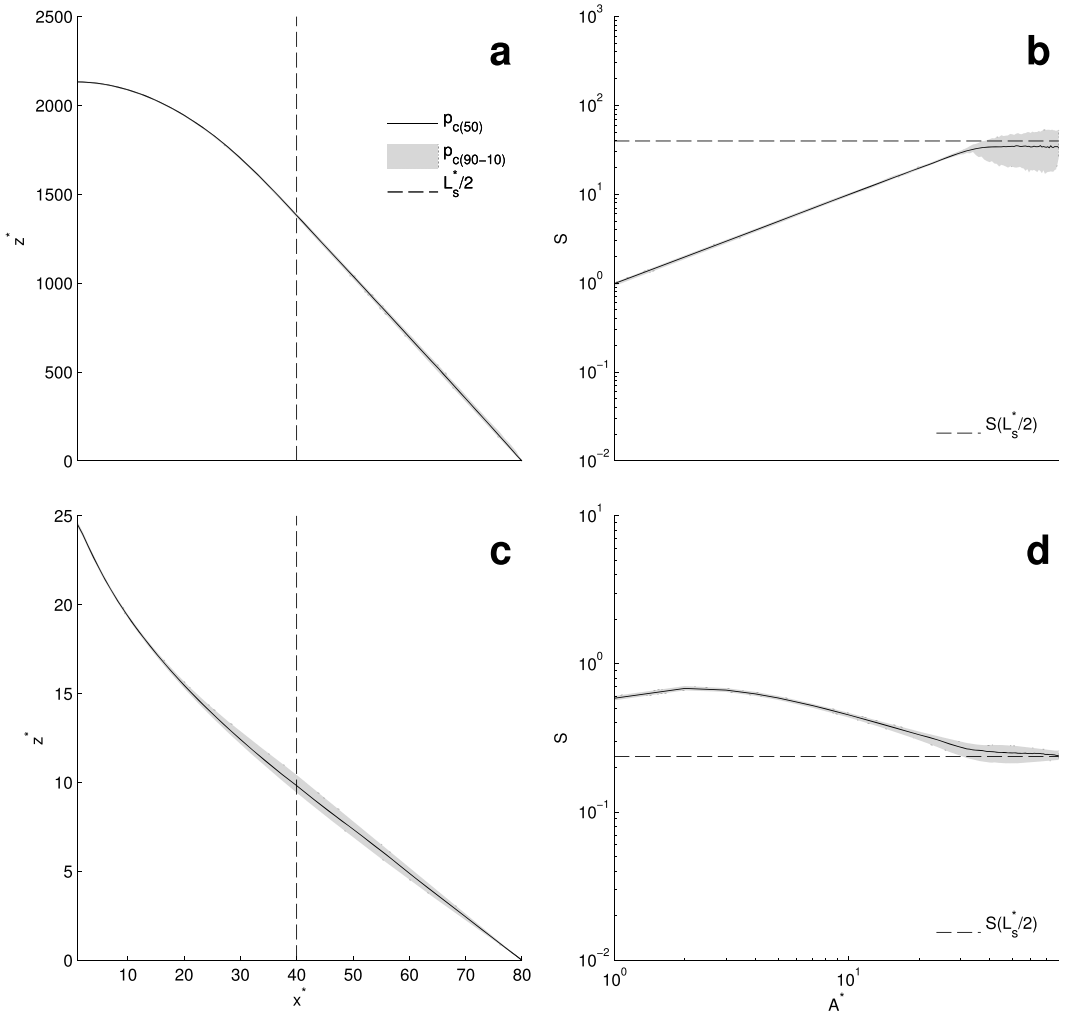

Figure 7. Topographic fluctuations in response to $S = R$ conditions. Topography and slope-area relations for 1-D simulations of (a, b) convex and (c, d) concave landscape as in the 1-D simulations in Figure 5. Dashed vertical line in Figures 7a and 7c marks the prescribed location where $S = R$. Dashed horizontal line in Figures 7b and 7d marks the prescribed value of R. Note that topographic fluctuations are centered at $S = R$.

associated with flow arrestment due to $S < R$ conditions. Note that $x^* < {}^dL_R^*$ and $x^* < {}^aL_R^*$ cannot overlap because $S < R$ conditions (i.e., $x^* < {}^dL_R^*$) can not occur where $S > R$ conditions prevail (i.e., $x^* < {}^aL_R^*$).

To numerically explore the topographic response to the occurrence of $S = R$ conditions within a landscape (i.e., $x^* > {}^dL_R^*$ or $x^* > {}^aL_R^*$), we simulate a simple case of an evolving landscape strip (of dimensions $\Delta x^* \times L_s^*$). In this experiment, we prescribe R as the steady state S value midway between each strip's divide and base level ($L_s^*/2$) for convex and concave topographies (Figure 7). To capture the topographic response to flow deposition and erosion at $S = R$, we suppressed the topographic fluctuations caused by stochastic flow generation. We do so by prescribing zero flows when $0 \le r_n < 0.01$, one flow when $0.01 \le r_n < 0.99$, and two flows when $0.99 \le r_n < 1$. With these arbitrarily chosen thresholds, single flows are generated in 98% of the cases within δt^* rather than 50% (section 2.5). We let the surface develop until a time-invariant relief is attained and continued to let it evolve while generating 200 temporally consequent modeled topographies. These topographies, generated every t^*, were then used to trace the temporal topographic fluctuations over the simulated surfaces. Figure 7 shows the relations between elevation, slope, and length from divide for these unstable topographies and demonstrates that a zone of prominent elevation fluctuations occurs at the proximity of $L_s^*/2$ (i.e., $L^* = 40$). Downslope of this point, the landscape has a time-averaged constant slope of $S \simeq R$. Model convergence in the context of these fluctuations is demonstrated in Figures S1 and S2.

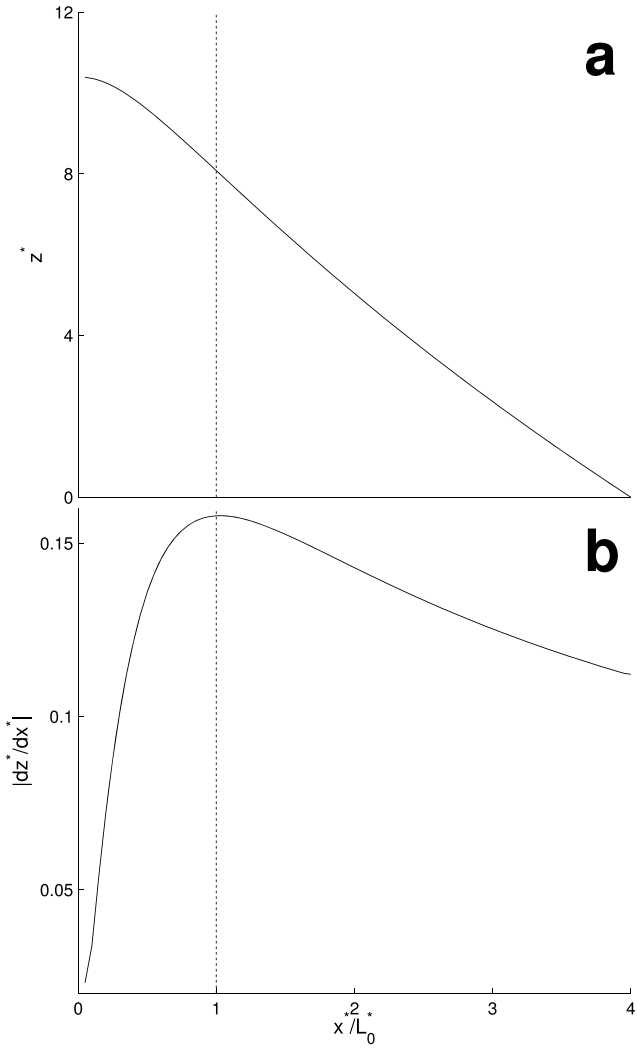

Figure 8. Transition from convex-up to concave-up topography as a function of the ratio between the distance from the divide (x^*) and the effective magnitude of localized surface disturbance (L_0^*, Table S1). (a) Simulated topography at steady state. The y axis shows the dimensionless surface elevation (z^*). (b) The same topography as in Figure 8a, only that now the y axis show the absolute value of the slope $|dz^*/dx^*|$ of the simulated topography. Note that the transition from convex-up to concave-up topography occurs at $x^*/L_0^* = 1$.

3.3. Transition From Convex to Concave Topography

In the proposed framework, the magnitude of sediment transport by local diffusive processes that form convex topography is determined by L_0, while that of nonlocal transport-limited processes that form concave topography is determined by the cumulative runout distance (L) of flows generated upslope. Thus, the sediment transport rate at a point reflects the additive effect of local and nonlocal processes, where the magnitude of L_0 versus L determines the extent of convex versus concave topography. For example, in the simple 1-D case (equation (15)) of $R = 0$, the setting of $L^* = L_0^*$ when $(x^*, y^*) = (x_0^*, y_0^*)$ sets the dimensionless sediment transport rate at this point to

$$q_a^*(x^*, y^*) = w^*(m+1)^{-1}\left[S(x^*, y^*)\right]^n \left(\left[L^*\left(x_0^*, y_0^*, x^*, y^*\right)\right]^{m+1} + L_0^{*m+1}\right) \tag{31}$$

where the term $([L^*(x_0^*, y_0^*, x^*, y^*)]^{m+1} + L_0^{*m+1})$ accounts for sediment transport by both local (L_0^*) and nonlocal (L^*) diffusion at each point in the landscape. To explore the relative effect of L_0^* and L^* on the geometry of the simulated landscape, we analyzed its impact on the transition from convex-up to concave-up topography over 1-D simulation of $R = 0$. Figure 8a shows that the resulting landscape profile is composed of a convex-up portion upslope of $x^*/L_0^* = 1$ and a concave-up one downslope of this point. Where $x^*/L_0^* = 1$ reflects the condition where the sediment transport rate due to local-diffusion is equal to that of nonlocal diffusion.

4. Discussion

4.1. Topographic Fluctuations in Response to Constrained Flow Runout Distance

The primary difference between the framework we propose and existing theory of landscape development by discretely generated flows [e.g., *Chase*, 1992; *Pratson and Coakley*, 1996; *Crave and Davy*, 2001; *Haff*, 2001] is the coupling between a flows' frequency, its interaction with the substrate over which it flows, and the runout distance. This coupling accounts for both the frequency of flow generation ($F(x_0, y_0, S, A)$), and the way in which flows traverse different landscape localities (captured by $f(x, y, x_0, y_0, \xi)$).

One interesting outcome of this coupling is that fluctuations in the transport processes that move material across the surface are produced when the runout distance of a flow is finite and contained within the model domain (section 3.2). Conceptually, areas of the landscape in which $x^* < {}^aL_R^*$ host $S > R$ conditions that produce stable, concave-up forms as transport capacity of geomorphic processes increases downslope, necessitating lower slopes to match the sediment supplied and forming concave-up topography. However, when $x^* > {}^aL_R^*$, $S < R$ conditions occur such that flows no longer run out and the sediment transport rate decreases. As slopes increase in response to this loss in transport capacity, flows once again sweep over the landscape. The alternation of transport processes and topographic conditions that is produced across this transition is captured by an increase in $pc(90-10)$ about this transition (Figures 7c and 7d). These fluctuations are associated with a time-averaged constant slope ($S \simeq R$) downslope of $x^* > {}^aL_R^*$ (Figures 7c and 7d). Similarly, when $x^* < {}^dL_R^*$, $S < R$ conditions prevail that produce stable, convex-up forms as transport processes act locally (section 3.2). However, when $x^* > {}^dL_R^*$, $S > R$ conditions occur such that flows runout for substantial distances and traverse downslope locations more frequently, causing an increase in sediment transport. As slopes reduce in response to this increase in transport capacity, flows once again arrest, thus producing a cyclic alternation of transport processes and topographic forms downslope of this transition (Figures 7a and 7b). Such episodic generation and arrest of flows qualitatively resembles the deposition and collapse of debris hollows [i.e., *Dietrich and Dunne*, 1978; *Reneau and Dietrich*, 1987; *Benda*, 1990]. Note that these fluctuations persist even when all other factors remain constant (and thus resemble the instabilities described by *Davy and Lague* [2009] at distances shorter than a disequilibrium distance), hence, demonstrating that topographic fluctuations may occur regardless of external forcings such as climate or tectonic activity.

The time-averaged constant slope value ($S \simeq R$) downslope of $x^* > {}^dL_R^*$ or $x^* > {}^aL_R^*$ suggests that changes in ${}^dL_R^*$ or ${}^aL_R^*$ in response to changes in R may cause changes in landscape relief. Thus, changes in flow runout distance in response to temporal variations in climate or substrate material may change the landscape relief.

4.2. Controls on the Topography of Simulated Landscapes

The numerical simulations we performed do not aim to capture the impact of a specific land-shaping process on the resulting topography but, instead, to demonstrate that simple constraints may underlie the formation of similar landforms across different physical environments. The variety of landscapes formed by the proposed framework is illustrated through a field diagram that schematically summarizes our analytical and numerical results over a nondimensional parameter space (Figure 9). This diagram demonstrates the impact of the nondimensional length from divide to outlet (L_s^*), R, and L_0^* on the form and topographic stability of 1-D landscapes produced by the proposed framework. The solid line that separates fields "a" and "b" describes the parameter combination for which $S = R$ exactly at L_s^* over a convex-up surface (equation (29)). A parameter combination that resides below this line, so that $S < R$ everywhere (field "a"), forms a stable convex-up landscape where flows do not run out so the landscape is entirely dominated by local diffusion (e.g., Figure 5). Above this line, in field "b," S approaches R somewhere within the landscape and topographic fluctuations arise (i.e., Figures 7a and 7b). The solid line that separates fields "c" and "d" describes the parameter combination at which $S = R$ exactly at L_s^* over a concave-up surface (equation (31)). A parameter combination that resides below this line (zone "d") forms a stable concave-up landscape where $S > R$ everywhere across the landscape so that long runout flows are everywhere generated and traverse the entire landscape (e.g., Figure 6). Above this line, in zone "c," S approaches R somewhere along a concave-up landscape (e.g., Figures 7c and 7d) so that long runout flows may periodically arrest creating topographic fluctuations (i.e., Figures 7c and 7d).

This field diagram also captures information about the impact of L_0^* on the resulting topography. As shown in section 2.3.1 and Figure 8, L_0^* determines the magnitude of local diffusive processes, and hence the extent of the convex-up portion of the landscape. It thus has a similar effect to that of a surface-wash efficacy variable [*Kirkby*, 1980; *Loewenherz*, 1991]. For example, as L_s^* decreases relative to L_0^*, an increasing portion of the

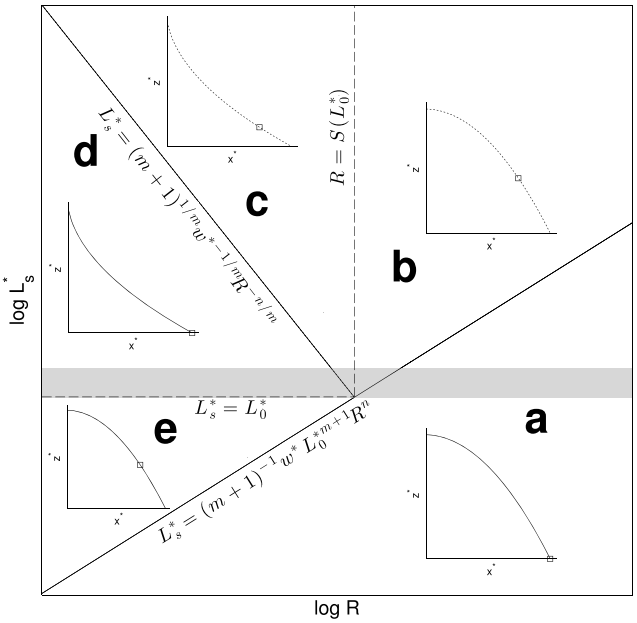

Figure 9. Field diagram showing the stability fields for convex-up and concave-up landscapes. Solid lines represent the stability criteria for concave-up and convex-up landscapes, respectively (i.e., equations (29) and (30)). Dashed lines mark L_s^* and R values at the intersection of the stability criteria. Inset figures show schematic topographic profile representative of the topographies simulated in each field. Solid lines in inset figures represent mathematically stable topographic profiles (fields a, d, e), dotted lines represent unstable profiles (fields b, c). Hollow squares at the middle and bottom of the topographic profile indicate that $S = R$ conditions occur upslope or downslope of L_s^*, respectively (this excludes $S = R$ occurrence at the convex-up portions upslope of L_0^* of mostly concave-up landscapes in fields c and d). Grey strip symbolizes the zone where L_s^* approaches L_0^*, so that the stability criteria for concave-up topography do not hold and the concave-up landscape in fields d and c has an increasing portion of convex-up topography.

concave-up topography in zone "d" becomes convex-up (e.g., Figure 8), so that when $L_0^* = L_s^*$ (dashed horizontal line separating fields "d" and "e") the entire landscape is convex. Thus, when $L_0^* > L_{sy}^*$ and $R < |S(L_0)|$ (field "e"), the landscape is entirely convex-up although long runout flows initiate downslope of $S = R$. Yet the consistent downslope increase in slope over this convex-up landscape prevents the sporadic arrest of these flows so that no topographic fluctuations arise. The dashed vertical line separating fields "b" and "c" shows the R value that equals the slope of a convex-up surface at a distance L_0^* from the drainage divide ($R = S(L_0^*)$). Thus, for a concave-up landscape located in field "c," an increase in R causes an upslope shift of the point $S = R$, so that when $R = S(L_0^*)$ (at the dashed line), the landscape is convex upslope of L_0^* and periodic arrest and generation of flows occur downslope of this line. A further increase in R expands the extent of the convex topography downslope of L_0^* and shifts the landscape into field "b." Note that the stability criterion for nonlocal diffusion (equation (30)) is derived only for the specific case of $L^* >> L_0^*$—this approximation breaks down as L_s^*/L_0^* decreases and approaches one, which is schematically depicted in Figure 9 as the gray zone where L_s^* on the order of L_0^*.

The hillslope forms simulated by the proposed framework demonstrate that it can produce a continuum of hillslope topographies that captures hillslope forms produced by linear (Figures 5a and 5b) and nonlinear (Figures 7a and 7b) diffusion [*Davis*, 1892; *Gilbert*, 1909; *Culling*, 1960; *Roering et al.*, 1999, 2001]. Such a continuum is also produced by nonlocal sediment transport models that rely on topographically dependent hop length statistics of particle motion [*Tucker and Bradley*, 2010; *Foufoula-Georgiou et al.*, 2010] rather than on a flow resistant coefficient such as R. Yet the continuum of landforms produced by the framework we propose also encompasses the channelized portion of the landscape (Figure 6).

The variety of landscapes formed within the different fields illustrated by Figure 9 demonstrates that when sediment transport is proportional to the frequency at which flows traverse the landscape, a simple constraint on flow dynamics, such as the flow resistance coefficient (R), may determine the shape of the landscape. Thus, the processes leading to the formation of a variety of natural landforms on Earth and other planets can potentially be generalized in terms of such simple constraints.

Our results also demonstrate that the stability criterion of *Smith and Bretherton* [1972], originally determined for rainfall and overland flow, does not depend on the synchronicity and spatial uniformity of flow initiation. Therefore, temporal summation of spatially discrete flows may have a similar effect to that of spatial integration of instantaneous flows (e.g., rainfall) and both can result in the formation of an undissected convex hillslopes or in the growth of perturbations along the surface and the establishment of branched valley networks, depending on the flow characteristics (further discussed in section 4.5).

4.3. Differences Between 1-D and 2-D Simulations and Their Effect on Landscape Analysis

Interestingly, the concavity value of simulated concave-up topography (Figure 6) varies appreciably between 1-D and 2-D simulations. While the 1-D simulations of concave-up landscapes (Figures 6a and 6b) display a concavity value similar to that prescribed by the m and n values in equation (7) (Table S1), the concavity of the 2-D simulation (Figures 6c and 6d) is about half of the prescribed value. This difference reflects the prescribed dependence of sediment transport on flow length (L), rather than drainage area (equation (7)). In 1-D simulations, flow length and drainage area are linearly proportional, so the prescribed flow length exponent m also holds when length is converted to area. In 2-D simulations, however, the nonlinear relations between flow length and drainage area are subsumed into the area exponent $M' = mh^{-1} + 1$ (equation (28)). Thus, at steady state, $S \propto A^{mh^{-1}n^{-1}}$, and because the value of h typically ranges between 1.4 and 2 [*Hack*, 1957; *Rigon et al.*, 1996], the resulting concavity is about half of the prescribed concavity value. This demonstrates that when the sediment transport rate of a particular process is proportional to flow runout distance rather than drainage area, the calibration of GTL parameters with empirical measurements of channel concavity should account for the geometry of the drainage basin as captured by parameters such as h [*Willet*, 2010].

The concavity values of convex-up topography are also sensitive to whether the simulations are 1-D or 2-D. While the 1-D convex-up simulations (Figures 5a and 5b) produce a concavity value of about −1, as expected for the linear diffusion end-member of the proposed framework (section 3.1), the 2-D simulations produce a concavity closer to zero where nodes of low drainage areas are associated with relatively high slope (Figure 5d versus Figure 5b). This difference arises from the roughness of the 2-D surface, an outcome of the spatiotemporal heterogeneity in sediment transport rate induced by the stochastic flow generation. This roughness causes temporal variations in flow pathways across the surface so that a node associated with steep slope and large upslope area at a given simulation time step may have smaller upslope area at the next time step. This results in areas of the model that have low drainage area and high slope that reduce the overall concavity in comparison to the 1-D case (Figures 5b and 5d). This phenomenon introduces an uncertainty into the standard analysis of digital elevation models (DEMs) in which the extent of the landscape that is dominated by linear-diffusion-like processes is determined from the transition between negative to zero concavity over slope-area plots [e.g., *Montgomery and Foufoula-Georgiou*, 1993; *Dietrich et al.*, 2003; *Tarolli and Dalla Fontana*, 2009]. The rough topography of low concavity values produced by low-frequency high-magnitude stochastic transport events may thus diverge from that produced by spatiotemporally continuous transport processes and lead to underestimation of the hillslope extent, and to overestimation of areas characterized by low concavity values such as those dominated by debris flows, landslides, or highly nonlinear hillslope diffusion [*Roering et al.*, 1999, 2001; *Tucker and Whipple*, 2002; *Stock and Dietrich*, 2003].

4.4. Topographic Response to Stochastic Flow Generation

High stochasticity in flow generation not only affects the convex portion of the landscape but also causes spatial patterns in the degree of topographic fluctuations in the channelized portion of the landscape. In simulations of concave-up landscapes (Figure 6), the magnitude of these fluctuations reduces downslope. This is because lower portions of the landscape are traversed by discrete flows generated over multiple upslope locations, such that the frequency at which discrete flows traverse landscape locations within the time period δt^* approaches $\bar{F} \times N_d$ as the upslope area increases (N_d is the number of upslope grid nodes that drain into a given node and $\bar{F}$ is the mean frequency of flow generation). Thus, while the frequency at which flows traverse upslope areas is highly dependent on the stochasticity of flow generation, the frequency at which flows traverse downslope locations is approximately constant and results in minor elevation fluctuations. This resembles submarine, subaerial, or Martian basins in which the upslope, small drainage area portions of basins have a large number of recent scarps associated with flow generation [*Lucchitta*, 1984; *Stock and Dietrich*, 2003, 2006; *Mitchell*, 2005] while their lower portions maintain a smooth-looking profile devoid of major topographic disturbances. These results demonstrate that the topographic stability of channels with large drainage areas can be produced within a landscape in which stochastically generated flows are the sole agent of transport. In this case, this stability may reflect a downslope averaging of the effects of upslope,

stochastically generated, discrete flows. It might be possible to distinguish landscapes dominated by stochastically generated flows using such observations of the spatial patterns of topographic fluctuations or by zero concavity conditions adjacent to drainage divides (as described in the previous section). Yet the variety of sediment transport processes that operate over natural landscapes (e.g., fluvial flows, soil creep, debris flows, rockfalls, and landslides) and the relatively low frequency of discrete flows such as debris flows (in comparison to the time scale of repeating observations) may make such distinction difficult to make.

4.5. Some Applications to Modeling and Analysis of Natural Landscapes and Processes

The numerical simulations we performed do not aim to capture the interaction of a specific land-shaping process with the topography or the topographic signature of a specific process. Yet the framework we propose can be used to investigate such specifics. This is enabled by the conceptual generality of equations (5) and (6), which makes them a place holder for GTLs and runout restrictions that describe various transport processes. Such substitution facilitates simulations that explore landscape response to such varying processes. For example, q_p (equation (5)) can be substituted with a GTL that describes sediment transport by debris flows [e.g., *Stock and Dietrich*, 2006], turbidity currents [e.g., *Traer et al.*, 2012], Martian granular flows [e.g., *Shinbrot et al.*, 2004], or rainfall-generated parcels of water (which can be viewed as discrete flows). Further, as demonstrated through the effect of $\bar{S}$ on the flow runout, the proposed framework can explicitly record upslope topographic and flow conditions and account for the impact of such nonlocal factors on the downslope flow dynamics (in the sense of *Stark et al.* [2009], *Furbish and Haff* [2010], *Foufoula-Georgiou et al.* [2010], *Tucker and Bradley* [2010], and *Falcini et al.* [2013]), such that upslope flow orientation, for example, can affect erosion and deposition at downslope locations [e.g., *Howard*, 1992; *Stock and Dietrich*, 2003, 2006]. This approach may therefore allow information about sediment transport by individual short-term events to be assimilated into an understanding of landscape dynamics that occur over large temporal and spatial scales.

In some cases, the parameters of the simplified GTL and runout constraint we propose (equations (7), (8), and (11)) can be calibrated with a specific process of interest which could facilitate first-order investigations of the interaction between this process and the landscape it forms. For example, R can be evaluated from the slope between the initiation and deposition points of a discretely generated flow such as a rockslide, landslide, or debris flow [e.g., *Heim*, 1932; *Dai and Lee*, 2002]. Likewise, the frequency of flow generation ($F(x_0, y_0, S, A)$) and its dependence on topographic parameters can be evaluated from topographic and time series analysis of markers of flows generation such as landslide or rockfall scarps [e.g., *Hovius et al.*, 1997; *Dai and Lee*, 2002]. Numerical investigation of landscape evolution based on such calibrated GTLs may provide first-order insights into the topographic impact of a process of interest and aid in the development of a GTL that represents this process more accurately.

The proposed framework uses simple formulations to produce convex, concave, and fluctuating topographies, as well as transitions between them. However, this flexibility does not mean that all landscapes can be modeled through such simple formulations. Earth's topography, for example, is shaped by multiple processes [e.g., *Luckman*, 1992; *Roering et al.*, 1999, 2001; *Tucker and Whipple*, 2002; *Stock and Dietrich*, 2003; *Dietrich et al.*, 2003] that are unlikely to be captured by a few simple formulations. Hence, an accurate model of the overall topographic impact of various types of discrete flows requires a composite approach where different GTLs and runout constraints are inserted in the appropriate place holders (i.e., equations (5) and (6)). This accounts for landscape evolution in response to sediment transport by multiple processes that operate simultaneously over the landscape.

While typical GTLs [*Dietrich et al.*, 2003] treat the spatial and temporal heterogeneity of natural processes by encapsulating their time-averaged behavior into an unvarying rate constant, the framework we propose facilitates explicit treatment of this heterogeneity (similar to *Chase* [1992], *Pratson and Coakley* [1996], *Crave and Davy* [2001], and *Haff* [2001]). This enables modeling of landscape development over time scales that are shorter than the time span assumed when processes are cast in time-averaged parameters. For example, in the case of local processes, the proposed framework enables explicit treatment of spatiotemporal variations in sediment transport through bioturbative processes such as gopher burrowing or tree fall [*Black and Montgomery*, 1991; *Norman et al.*, 1995; *Roering et al.*, 2001; *Gabet et al.*, 2003]. Thus, field-measured parameters such as the spatiotemporal distribution of tree-fall events and their magnitude and direction can be treated, and the landscape's response to these parameters can be simulated. The proposed framework may thus facilitate prediction of short-term topographic response to abrupt climatic, biogenic, and anthropogenic perturbations.

In the case of nonlocal processes, the explicit treatment of spatiotemporally discrete flows may also aid in capturing the topographic effect of phenomena such as discrete precipitation events. Although discharge- and frequency-dependent sediment transport mechanisms are not necessarily exclusive (i.e., individual sediment-carrying parcels of water can be viewed as discrete flows, such that downslope increase in discharge can be akin to downslope increase in the frequency at which such flows traverse a given locations), these mechanisms can differ even in a simple fluvial scenario. For example, discharge-dependent GTLs (e.g., equation (4)) typically assume that upslope drainage area determines the discharge and the associated flow depth (assuming some channel geometry) which affect the flow dynamics and sediment transport capacity [e.g., *Howard*, 1980; *Willgoose et al.*, 1991a; *Howard*, 1994; *Whipple and Tucker*, 2002]. However, while this holds when precipitation is uniformly distributed over a basin, it may differ when the same amount of precipitation is distributed discretely in space and time [e.g., *Tucker and Bras*, 2000; *Snyder et al.*, 2003]. When the time interval between discrete flow-generating precipitation events is longer than their duration, flows generated at different parts of a basin do not coalesce downslope to form a high-discharge event. Instead, multiple-flow events of low discharge may flow through the basin outlet. Thus, although the same volume of water may flow through the basin over some time period used to average the landscape response, the overall volume of sediment carried by the water in these uniformly distributed and discrete cases may be different. This difference reflects the nonlinear dependence between sediment transport rate and discharge [*Tucker and Bras*, 2000; *Snyder et al.*, 2003]), such that the quantity of sediment transported by a high-discharge event can be greater than that carried by the same discharge partitioned into several smaller events and summed up. The dependence between topographic response and drainage area may thus be different between these two scenarios, and accounting for the number of flow events that traverse different locations within a basin, as well as their interactions (captured in ξ), may be essential to properly capture the topographic response to these events. The proposed framework may therefore provide a convenient template for simulating the topographic impact of phenomena such as desert floods in a manner that accounts for the high spatiotemporal variation [e.g., *Sharon*, 1972] in the precipitation events that generate these floods. The impact of upslope infiltration and evaporation [e.g., *Dahan et al.*, 2008] on the runout distance of these floods may be accounted for by utilizing the nonlocal capability of the proposed framework.

4.6. Limitations and Scope

While the general framework we propose in equations (5) and (6) aims to address the ubiquity of hillslopes and channel networks across different physical environments (dominated by both uniformly distributed and discrete flows), some fundamental questions associated with this ubiquity are yet to be answered. For example, we do not address the question of why and how different processes that operate in disparate physical environments are characterized by a nonlinear increase in sediment transport capacity (in excess of sediment supply) per unit area.

The proposed framework is primarily cast in terms of "transport-limited" conditions (equation (2)) to demonstrate that hillslopes and channel networks can be viewed as end-member morphologies along a continuum controlled by the landscape and flow runout lengths (Figure 9 and equations (29) and (30)). While a modification of the framework can describe "detachment-limited" channel erosion (section 2.3.2) it does not reconcile "detachment-limited" erosion and hillslope formation as part of the same continuum (i.e., Figure 9 does not include detachment-limited conditions). Note that the flow runout length we use describes the distance to which an individual flow may progress downslope (with or without sediment), and that it differs from the "transport distance" used by *Kooi and Beaumont* [1994, 1996] and *Crave and Davy* [2001].

The energy balance in equation (11) assumes a constant flow mass and in this way is inconsistent with the fact that flow mass may change downslope as it deposits and entrains mass from the bed (equation (7)). This inconsistency is an outcome of the complex momentum exchange between the flow and its surrounding [*Iverson*, 1997] (see section 2.3.3). We allow and acknowledge this inconsistency in our illustrative models, but note that an energy balance that couples the runout of the flow to mass and momentum would be a fruitful addition to this work. Note that equation (11) is substituted into the runout distance constraint (equation (6)) to provide a simple illustration of the effect of limited runout distance and that other formulations that describe specific processes can be substituted into equation (6) instead.

The computation time of landscape evolution models is typically constrained by $O(N \log N)$ operations or less [e.g., *Braun and Willett*, 2013; *Richardson et al.*, 2014], which is more efficient than that of the proposed framework ($O(N^2)$). This computation time inefficiency is an outcome of tracing individual flows to determine their

runout distance. However, because in each time step the flows run over the topography formed in the previous time step, and because we do not consider flow coalescence, individual flows can be treated independently such that parallelizing this framework is straightforward. Such parallelization, however, is impossible in simulations that seek to explore the effect of flow coalescence (or other forms of interaction between flows) because in that case flows are no longer independent and the quantity of sediment transported by all flows can not be computed through a simple summation.

Although flow coalescence can be accounted for by the state variable ξ, for simplicity and computational expediency this study does not explore such processes. One way to account for flow coalescence is through a probabilistic approach, where, for example, the likelihood of flow coalescence increases with the number of flows that traverse a pixel within a time step. An alternate, more physical approach can be applied for flows of known velocity, spatial dimensions, and generation time, such that flows and their coalescence can be explicitly traced in space and time. As noted in the previous paragraph, accounting for flow coalescence will increase the model's computational load.

The numerical implementation generates flows from pixel-sized locations (similar to *Chase* [1992], *Pratson and Coakley* [1996], *Crave and Davy* [2001], and *Haff* [2001]) and routes them downslope using a single flow direction routing scheme, thus introducing some gridded imprint on the evolving landscape. This imprint can be reduced by enabling generation of multipixel flows (which can be easily prescribed into the existing framework), and using multiple direction routing scheme [e.g., *Freeman*, 1991; *Tarboton*, 1997; *Shelef and Hilley*, 2013]. Using such routing schemes, however, will increase computational load because each portion of a bifurcating flow will have to be traced to determine the conditions for its arrest.

5. Summary

Branched valley networks and undissected hillslopes are observed across disparate physical environments, where both discrete and uniformly distributed flows shape the landscape. This ubiquity suggests that common criteria exists for the formation of these landforms, regardless of the physical conditions and types of flows that shape these landscapes. This study formulates an analytical framework that casts the conditions for channel networks and hillslope formation by discrete flows in general terms that are likely common to these different environments. This framework describes changes in surface topography expected to arise from sediment transport events that are discrete in space and time. The amount of sediment carried through each point in the landscape depends on topographic attributes, as well as the frequency at which this point is traversed by discrete flows, a frequency that is in turn dependent on the conditions for flow generation and arrest (described here by a simple energy balance). These dependencies explicitly link the time scale of sediment transport to the topography and flow dynamics that control flow generation and arrest, and thus offer an alternative to the spatially unvarying rate constant typically used in GTLs. Further, treating flows as discrete entities facilitates incorporation of nonlocal impacts on the sediment transport rate at a point, as well as explicit treatment of natural process whose behavior is stochastic over short time scales. Thus, the proposed framework provides a rational means of modeling natural flows whose dynamics and frequency of occurrence may vary both spatially and temporally.

We explore this framework through a simple, posited GTL and a flow runout constraint, which together describe flows that differ in their runout distance and in the way their transport capacity changes downslope. We use this GTL and runout constraint to show that the rate of sediment transport by multiple individual flows may or may not depend on a drainage area term (akin to that used in GTLs describing fluvial processes) depending on their flow characteristics and to analytically and numerically demonstrate that specific end-members implied by the proposed framework produce branched channel networks and undissected hillslopes, as well as topographic fluctuations that persist even when all other factors remain constant through time. The framework's structure facilitates substitution of these posited GTL and runout constraints with expressions that are more representative of specific processes. Our results also demonstrate that the stability criteria of *Smith and Bretherton* [1972], originally determined for rainfall and overland flow, do not depend on the synchronicity and uniformity of flow initiation, in that temporal summation of spatially discrete flows (with $M' > 0$, $R < S$, section 3.1.2) may result in topographic instability and perturbation growth akin to those produced from spatial integration of instantaneous flows (e.g., distributed rainfall). Hence, both can result in the formation of hillslopes or in establishment of branched valley networks, depending on the flow characteristics.

Notation

a Coordinate of a given location in 1-D space [L^2].
a_0 Coordinate of flow generation location in 1-D space [L^2].
A Drainage area [L^2].
A' Integration boundary that reflects the area that drains into a point [L^2].
D Rate constant for diffusive GTL [L^2t^{-1}].
D' Rate constant for diffusive processes attained through combination of parameters from the proposed framework [L^2t^{-1}].
dx, dy Infinitesimal length increments [L].
$\dot{E}$ Erosion rate [Lt^{-1}].
F Frequency of flow generation [$L^{-2}t^{-1}$].
$\bar{F}$ Mean frequency of flow generation [$L^{-2}t^{-1}$].
F_0 Reference frequency of flow generation [$L^{-2}t^{-1}$].
g Gravitation acceleration [$L\ t^{-2}$].
h Exponent relating maximal flow length and drainage area [].
i, j Grid indices [].
$i0, j0$ Grid indices of nodes where flows are generated [].
k Rate constant for nonlocal diffusive fluvial sediment transport-limited GTL [$L^{2-2m}\ t^{-1}$].
k_{df} Rate constant for a portion of discrete flow [$L^{\ 2-m}\ t^{-1}$].
k_a Coefficient relating maximal flow length and flow area [L^{2-h}] .
k_A Rate constant for discrete flows when length is converted to area [$L^{\ 2-2m}\ t^{-1}$].
K Representation of the grouped coefficients $k_{df}TF$ [L^mt^{-1}].
l_c Characteristic length [L].
L Flow route length [L].
L_0 Finite length correlative to momentum provided by localized surface disturbance [L].
m' Drainage area exponent in the context of traditional GTLs [].
m Flow route length exponent [].
M Flow mass [M].
M' Area exponent [].
n' Surface slope exponent in the context of traditional GTLs [].
n Surface slope exponent in the context of discrete flows [].
$\bar{n_f}$ Number of discrete flows generated within dimensionless area Δx^*, Δy^* and time interval.
N Number of flows that traverse a location [].
N_d Number of upslope grid nodes that drain into a given node [].
p_c Given percentile of a topographic metric (elevation, slope) extracted from N number of simulations [].
q_a Sediment transport rate per unit width summed for all flows that traverse a point [$L^2\ t^{-1}$].
${}^sq_a$ Sediment transport rate per unit width summed for all flows that traverse a point according to specific formulation in equation (8) [$L^2\ t^{-1}$].
q_{dif} Sediment transport rate per unit width for diffusive processes [$L^2\ t^{-1}$].
q_n Sediment transport rate per unit width for nonlocal diffusive processes [$L^2\ t^{-1}$].
q_p Sediment transport rate per unit width of a portion of a flow at a point [$L^2\ t^{-1}$].
${}^sq_p$ Sediment transport rate per unit width of a portion of a flow according to specific formulation in equation (7) [$L^2\ t^{-1}$].
q_{pe} Erosion rate for a portion of a flow according to specific formulation in equation (9) [$L\ t^{-1}$].
q_s Sediment transport rate per unit width that is required to maintain steady state [$L^2\ t^{-1}$].
q_w Sediment transport rate per unit width [$L^2\ t^{-1}$].
r_n Random number between zero and one that determines the number of flows generated at each grid node [].
R Flow resistance coefficient [].
S Surface slope [].
S_{vx} Steady state slope over 1-D convex-up landscape [].
S_{ve} Steady state slope over 1-D concave-up landscape [].
$\bar{S}$ Mean slope along flow route [].

t Time [t].
t_c Reference time interval [t].
T_d Flow duration [t].
u Rock uplift rate [L t^{-1}].
u_0 Reference rock uplift rate [L t^{-1}].
w Width of a landscape strip [L].
W Channel width [L].
x, y Spatial coordinates [L].
x_0, y_0 Coordinates of flow generation location [L].
z Elevation [m].
ΔH Finite elevation difference [L].
ΔL Finite flow route length difference [L].
Δx Distance between grid nodes in x direction [L].
Δy Distance between grid nodes in y direction [L].
Δ_e Grid node spacing [L].
∇ Divergence operator [L^{-1}].
θ Channel concavity [].
ρ_r Rock density [M L^{-3}].
ρ_s Sediment density [M L^{-3}].
ξ State variable that accounts for flow characteristics (e.g., geometry, rheology) [].
ζ A function that captures the dependence of flow runout distance on flow properties and topography.
A^* Dimensionless drainage area [].
A_i^* Nondimensional drainage area of the ith node of a given grid [].
$\bar{A}^*$ Mean drainage area for a grid [].
dx^*, dy^* Nondimensional infinitesimal length increments[].
F^* Dimensionless frequency of flow generation [].
k_{df}^* Dimensionless rate constant for a portion of discrete flow [].
L^* Dimensionless flow route length [].
L_0^* Dimensionless finite length correlative to momentum provided by localized surface disturbance [].
${}^aL_R^*$ Dimensionless critical length from divide for nonlocal processes [].
${}^dL_R^*$ Dimensionless critical length from divide for diffusive processes [].
L_s^* Dimensionless simulation length from divide to a constant elevation boundary [].
L_{sy}^* Dimensionless simulation length in the y direction [].
L_{sx}^* Dimensionless simulation length in the x direction [].
q_a^* Dimensionless sediment transport rate per unit width summed for all flows that traverse a point [].
q_d^* Discrete dimensionless sediment transport rate per unit width summed for all flows that traverse a point [].
q_p^* Dimensionless sediment transport rate per unit width of a portion of a flow at a point [].
q_w^* Dimensionless sediment transport rate per unit width [].
t^* Dimensionless model time [].
T^* Dimensionless flow duration [].
u^* Dimensionless uplift [].
w^* Dimensionless width of 1-D surface [].
W^* Dimensionless channel width [].
x^*, y^* Dimensionless spatial coordinates [].
x_0^*, y_0^* Dimensionless coordinates of flow generation location [].
x_{i0}^*, y_{j0}^* Dimensionless discrete coordinates of flow generation location [].
x_i^*, y_j^* Dimensionless discrete coordinates [].
$x_{i\pm1/2}^*, y_{j\pm1/2}^*$ Dimensionless discrete coordinates between (x_i^*, y_j^*) and $(x_i^* \pm \Delta x^*/2, y_j^* \pm \Delta y^*/2)$ [].
x_n^*, y_m^* Dimensionless discrete coordinates of the node in the direction of steepest descent from (x_i^*, y_j^*) [].
x_{in}^*, y_{jm}^* Dimensionless discrete coordinates midway between (x_i^*, y_j^*) and (x_n^*, y_m^*) [].

z^* Dimensionless elevation [].
$\bar{z^*}$ Mean dimensionless elevation over a grid [].
$z^*_{i,j}$ Discrete dimensionless elevation at the node (i, j) [].
Δx^* Dimensionless distance between grid nodes in x direction [].
Δy^* Dimensionless distance between grid nodes in y direction [].
Δ^*_{nm} Dimensionless distance between (x_i, y_j) and (x_n, y_m) [].
Δt^* Dimensionless model time step [].
δt^* Prescribed dimensionless time increment that ensures $\bar{n_f} = 1$ [].
Δ^*_e Dimensionless grid node spacing [].
∇^* Dimensionless divergence operator [].
∇^*_d Discrete dimensionless divergent operator [].
ρ^* Dimensionless density [].

Acknowledgments
Data supporting our analysis are contained as tables and figures within the manuscript and supporting information. For specific questions regarding the data please contact Eitan Shelef (shelef@pitt.edu). We would like to thank J.M. Buffington, A. Densmore, J.D. Pelletier, S. Carretier, and two anonymous reviewers for insightful and thorough comments that helped in improving this manuscript. We also thank S. Johnstone, S. Moon, and A. Bachan-Dovrat for valuable discussions and early review of this manuscript. E.S. thanks Stanford's Lieberman Fellowship for its generous support.

References

Aharonson, O., M. T. Zuber, D. H. Rothman, N. Schorghofer, and K. X. Whipple (2002), Drainage basins and channel incision on Mars, *Proc. Natl. Acad. Sci. U.S.A.*, *99*(4), 1780–1783.
Benda, L. (1990), The influence of debris flows on channels and valley floors in the Oregon Coast Range, USA, *Earth Surf. Processes Landforms*, *15*(5), 457–466.
Black, B. A., J. T. Perron, D. M. Burr, and S. A. Drummond (2012), Estimating erosional exhumation on Titan from drainage network morphology, *J. Geophys. Res.*, *117*, E08006, doi:10.1029/2012JE004085.
Black, T. A., and D. R. Montgomery (1991), Sediment transport by burrowing mammals, Marin County, California, *Earth Surf. Processes Landforms*, *16*(2), 163–172.
Booth, A. M., and J. J. Roering (2011), A 1-D mechanistic model for the evolution of earthflow-prone hillslopes, *J. Geophys. Res.*, *116*, F04021, doi:10.1029/2011JF002024.
Braun, J., and S. D. Willett (2013), A very efficient O(n), implicit and parallel method to solve the stream power equation governing fluvial incision and landscape evolution, *Geomorphology*, *180*, 170–179.
Carson, M. A., and M. J. Kirkby (1972), *Hillslope Form and Process*, 475 pp., Cambridge Univ. Press, Cambridge, U. K.
Chase, C. G. (1992), Fluvial landsculpting and the fractal dimension of topography, *Geomorphology*, *5*(1), 39–57.
Chirico, G., A. Western, R. Grayson, and G. Blöschl (2005), On the definition of the flow width for calculating specific catchment area patterns from gridded elevation data, *Hydrol. Processes*, *19*(13), 2539–2556.
Costa-Cabral, M., and S. Burges (1994), Digital Elevation Model Networks (DEMON): A model of flow over hillslopes for computation of contributing and dispersal areas, *Water Resour. Res.*, *30*(6), 1681–1692, doi:10.1029/93WR03512.
Crave, A., and P. Davy (2001), A stochastic "precipiton" model for simulating erosion/sedimentation dynamics, *Comput. Geosci.*, *27*(7), 815–827.
Culling, W. (1960), Analytical theory of erosion, *J. Geol.*, *68*(3), 336–344.
Curry, A. M. (1999), Paraglacial modification of slope form, *Earth Surf. Processes Landforms*, *24*(13), 1213–1228.
Dahan, O., B. Tatarsky, Y. Enzel, C. Kulls, M. Seely, and G. Benito (2008), Dynamics of flood water infiltration and ground water recharge in hyperarid desert, *Ground Water*, *46*(3), 450–461.
Dai, F., and C. Lee (2002), Landslide characteristics and slope instability modeling using GIS, Lantau Island, Hong Kong, *Geomorphology*, *42*(3), 213–228.
Davis, W. M. (1892), The convex profile of bad-land divides, *Science*, *20*(508), 245.
Davy, P., and D. Lague (2009), Fluvial erosion/transport equation of landscape evolution models revisited, *J. Geophys. Res.*, *114*, F03007, doi:10.1029/2008JF001146.
Dietrich, W. E., and T. Dunne (1978), Sediment budget for a small catchment in mountainous terrain, *Z. Geomorphol.*, *29*, 191–206.
Dietrich, W. E., and J. T. Perron (2006), The search for a topographic signature of life, *Nature*, *439*(7075), 411–418.
Dietrich, W. E., D. G. Bellugi, L. S. Sklar, J. D. Stock, A. M. Heimsath, and J. J. Roering (2003), Geomorphic transport laws for predicting landscape form and dynamics, in *Prediction in Geomorphology, Geophys. Monogr. Ser.*, vol. 135, edited by P. Wilcock and R. Iverson, pp. 103–132, AGU, Washington, D. C., doi:10.1029/135GM09.
Dunne, T. (1980), Formation and controls of channel networks, *Prog. Phys. Geogr.*, *4*(2), 211–239.
Dunne, T., and B. F. Aubry (1986), Evaluation of Horton's theory of sheetwash and rill erosion on the basis of field experiments, in *Hillslope Processes*, edited by A. D. Abrahams, pp. 31–53, Allen and Unwin, Winchester, Mass.
England, P., and P. Molnar (1990), Surface uplift, uplift of rocks, and exhumation of rocks, *Geology*, *18*(12), 1173–1177.
Falcini, F., E. Foufoula-Georgiou, V. Ganti, C. Paola, and V. Voller (2013), A combined nonlinear and nonlocal model for topographic evolution in channelized depositional systems, *J. Geophys. Res. Earth Surface*, *118*, 1617–1627, doi:10.1002/jgrf.20108.
Flint, J. (1974), Stream gradient as a function of order, magnitude, and discharge, *Water Resour. Res.*, *10*(5), 969–973, doi:10.1029/WR010i005p00969.
Flint, J.-J. (1973), Experimental development of headward growth of channel networks, *Geol. Soc. Am. Bull.*, *84*(3), 1087–1094.
Foufoula-Georgiou, E., V. Ganti, and W. Dietrich (2010), A nonlocal theory of sediment transport on hillslopes, *J. Geophys. Res.*, *115*, F00A16, doi:10.1029/2009JF001280.
Freeman, T. (1991), Calculating catchment area with divergent flow based on a regular grid, *Comput. Geosci.*, *17*(3), 413–422.
Furbish, D. J., and P. K. Haff (2010), From divots to swales: Hillslope sediment transport across diverse length scales, *J. Geophys. Res.*, *115*, F03001, doi:10.1029/2009JF001576.
Gabet, E. J., O. Reichman, and E. W. Seabloom (2003), The effects of bioturbation on soil processes and sediment transport, *Annu. Rev. Earth Planet. Sci.*, *31*(1), 249–273.
Gilbert, G. K. (1877), *Report on the Geology of the Henry Mountains*, U. S. Geog. and Geol. Surv. of the Rocky Mt. Reg. (J. W. Powell), Govt. Print. Off., 170 p., Washington, D. C.
Gilbert, G. K. (1909), The convexity of hilltops, *J. Geol.*, *17*(4), 344–350.

Hack, J. (1957), Studies of longitudinal stream profiles in Virginia and Maryland, *U.S. Geol. Surv. Prof. Pap.*, *292*, 45–97.
Haff, P. K. (2001), Waterbots, in *Landscape Erosion and Evolution Modeling*, edited by R. S. Harmon and W. W. Doe, pp. 239–275, Springer, New York.
Heim, A. (1932), Der bergsturz von elm, *Deustch. Geol. Gazell. Z.*, *34*, 74–115.
Horton, R. (1945), Erosional development of streams and their drainage basins; hydrophysical approach to quantitative morphology, *Geol. Soc. Am. Bull.*, *56*(3), 275–370.
Hovius, N., C. P. Stark, and P. A. Allen (1997), Sediment flux from a mountain belt derived by landslide mapping, *Geology*, *25*(3), 231–234.
Howard, A., and G. Kerby (1983), Channel changes in badlands, *Geol. Soc. Am. Bull.*, *94*(6), 739–752, doi:10.1130/0016-7606(1983)94<739:CCIB>2.0.CO;2.
Howard, A. D. (1971), Simulation model of stream capture, *Geol. Soc. Am. Bull.*, *82*(5), 1355–1376, doi:10.1130/0016-7606(1971)825B1355:SMOSC5D2.0.CO;2.
Howard, A. D. (1980), Thresholds in river regimes, in *Thresholds in Geomorphology*, edited by D. R. Coates and J. D. Vitek, pp. 227–258, Allen and Unwin, Concord, Mass.
Howard, A. D. (1992), Modeling channel migration and floodplain sedimentation in meandering streams, in *Lowland Floodplain Rivers: Geomorphological Perspectives*, edited by P. A. Carling and G. E. Petts, pp. 1–41, Wiley, Chichester, England.
Howard, A. D. (1994), A detachment-limited model of drainage basin evolution, *Water Resour. Res.*, *30*(7), 2261–2286, doi:10.1029/94WR00757.
Howard, A. D. (1998), Long profile development of bedrock channels: Interaction of weathering, mass wasting, bed erosion, and sediment transport, in *Rivers Over Rock: Fluvial Processes in Bedrock Channels, Geophys. Monogr. Ser.*, vol. 107, edited by K. J. Tinkler and E. E. Wohl, pp. 297–319, AGU, Washington, D. C.
Hsu, K. J. (1975), Catastrophic debris streams (sturzstroms) generated by rockfalls, *Geol. Soc. Am. Bull.*, *86*(1), 129–140.
Iverson, R. M. (1997), The physics of debris flows, *Rev. Geophys.*, *35*(3), 245–296.
Kirkby, M. (1980), The stream head as a significant geomorphic threshold, in *Thresholds in Geomorphology*, edited by D. R. Coates and J. D. Vitek, pp. 53–73, Allen and Unwin, Concord, Mass.
Kirkby, M. J. (1971), Hillslope process-response models based on the continuity equation, *Inst. Br. Geogr. Spec. Publi.*, *3*, 15–30.
Kooi, H., and C. Beaumont (1994), Escarpment evolution on high-elevation rifted margins: Insights derived from a surface processes model that combines diffusion, advection, and reaction, *J. Geophys. Res.*, *99*(B6), 12,191–12,209, doi:10.1029/94JB00047.
Kooi, H., and C. Beaumont (1996), Large-scale geomorphology: Classical concepts reconciled and integrated with contemporary ideas via a surface processes model, *J. Geophys. Res.*, *101*(B2), 3361–3386.
Leopold, L., and T. Maddock (1953), The hydraulic geometry of stream channels and some physiographic implications, *U.S. Geol. Surv. Prof. Pap.*, *252*, 57.
Loewenherz, D. (1991), Stability and the initiation of channelized surface drainage: A reassessment of the short wavelength limit, *J. Geophys. Res.*, *96*(B5), 8453–8464, doi:10.1029/90JB02704.
Lucchitta, B. K. (1984), Ice and debris in the fretted terrain, Mars, *J. Geophys. Res.*, *89*(S02), B409–B418.
Luckman, B. H. (1977), The geomorphic activity of snow avalanches, *Geogr. Ann., Ser. A*, *59*(1), 31–48.
Luckman, B. H. (1978), Geomorphic work of snow avalanches in the Canadian Rocky Mountains, *Arct. Alp. Res.*, *10*(2), 261–276.
Luckman, B. H. (1992), Debris flows and snow avalanche landforms in the Lairig Ghru, Cairngorm Mountains, Scotland, *Geogr. Ann., Ser. A*, *74*, 109–121.
McGregor, B., W. L. Stubblefield, W. B. Ryan, and D. C. Twichell (1982), Wilmington Submarine Canyon: A marine fluvial-like system, *Geology*, *10*(1), 27–30.
McGuire, L. A., and J. D. Pelletier (2013), Relationships between debris fan morphology and flow rheology for wet and dry flows on Earth and Mars: A numerical modeling investigation, *Geomorphology*, *197*, 145–155, doi:10.1016/j.geomorph.2013.05.005.
Mitchell, N. (2005), Interpreting long-profiles of canyons in the USA Atlantic continental slope, *Mar. Geol.*, *214*(1), 75–99, doi:10.1016/j.margeo.2004.09.005.
Mitchell, N. C. (2004), Form of submarine erosion from confluences in Atlantic USA continental slope canyons, *Am. J. Sci.*, *304*(7), 590–611.
Mitchell, N. C. (2006), Morphologies of knickpoints in submarine canyons, *Geol. Soc. Am. Bull.*, *118*(5–6), 589–605.
Mitchell, N. C., D. G. Masson, A. B. Watts, M. J. R. Gee, and R. Urgeles (2002), The morphology of the submarine flanks of volcanic ocean islands: A comparative study of the Canary and Hawaiian hotspot islands, *J. Volcanol. Geotherm. Res.*, *115*(1–2), 83–107.
Montgomery, D. R., and J. M. Buffington (1997), Channel-reach morphology in mountain drainage basins, *Geol. Soc. Am. Bull.*, *109*(5), 596–611.
Montgomery, D. R., and E. Foufoula-Georgiou (1993), Channel network source representation using digital elevation models, *Water Resour. Res.*, *29*(12), 3925–3934, doi:10.1029/93WR02463.
Moore, I., and R. Grayson (1991), Terrain-based catchment partitioning and runoff prediction using vector elevation data, *Water Resour. Res.*, *27*(6), 1177–1191, doi:10.1029/91WR00090.
Norman, S. A., R. J. Schaetzl, and T. W. Small (1995), Effects of slope angle on mass movement by tree uprooting, *Geomorphology*, *14*(1), 19–27, doi:10.1016/0169-555X(95)00016-X.
Perron, J., W. Dietrich, and J. Kirchner (2008), Controls on the spacing of first-order valleys, *J. Geophys. Res.*, *113*, F04016, doi:10.1029/2007JF000977.
Perron, J., P. Richardson, K. Ferrier, and M. Lapôtre (2012), The root of branching river networks, *Nature*, *492*(7427), 100–103, doi:10.1038/nature11672.
Pratson, L. F., and B. J. Coakley (1996), A model for the headward erosion of submarine canyons induced by downslope-eroding sediment flows, *Geol. Soc. Am. Bull.*, *108*(2), 225–234.
Prosser, I., and P. Rustomji (2000), Sediment transport capacity relations for overland flow, *Prog. Phys. Geogr.*, *24*(2), 179–193.
Reneau, S. L., and W. E. Dietrich (1987), The importance of hollows in debris flow studies; Examples from Marin County, California, *Rev. Eng. Geol.*, *7*, 165–180.
Richardson, A., C. N. Hill, and J. T. Perron (2014), IDA: An implicit, parallelizable method for calculating drainage area, *Water Resour. Res.*, *50*, 4110–4130, doi:10.1002/2013WR014326.
Rigon, R., I. Rodriguez-Iturbe, A. Maritan, A. Giacometti, D. G. Tarboton, and A. Rinaldo (1996), On Hack's law, *Water Resour. Res.*, *32*(11), 3367–3374, doi:10.1029/96WR02397.
Rodríguez-Iturbe, I., A. Rinaldo, R. Rigon, R. Bras, A. Marani, and E. Ijjász-Vásquez (1992), Energy dissipation, runoff production, and the three-dimensional structure of river basins, *Water Resour. Res.*, *28*(4), 1095–1103, doi:10.1029/91WR03034.
Roering, J. J., J. W. Kirchner, and W. E. Dietrich (1999), Evidence for nonlinear, diffusive sediment transport on hillslopes and implications for landscape morphology, *Water Resour. Res.*, *35*(3), 853–870, doi:10.1029/1998WR900090.

Roering, J. J., J. W. Kirchner, L. S. Sklar, and W. E. Dietrich (2001), Hillslope evolution by nonlinear creep and landsliding: An experimental study, *Geology*, *29*(2), 143–146.
Scheidegger, A. E. (1973), On the prediction of the reach and velocity of catastrophic landslides, *Rock Mech.*, *5*(4), 231–236.
Sharon, D. (1972), The spottiness of rainfall in a desert area, *J. Hydrol.*, *17*(3), 161–175.
Shelef, E., and G. E. Hilley (2013), Impact of flow routing on catchment area calculations, slope estimates, and numerical simulations of landscape development, *J. Geophys. Res. Earth Surface*, *118*, 2105–2123, doi:10.1002/jgrf.20127.
Shelef, E., and G. E. Hilley (2014), Symmetry, randomness, and process in the structure of branched channel networks, *Geophys. Res. Lett.*, *41*(10), 3485–3493, doi:10.1002/2014GL059816.
Shinbrot, T. (2007), Delayed transitions between fluid-like and solid-like granular states, *Eur. Phys. J. E*, *22*(3), 209–217.
Shinbrot, T., N.-H. Duong, L. Kwan, and M. Alvarez (2004), Dry granular flows can generate surface features resembling those seen in Martian gullies, *Proc. Natl. Acad. Sci. U.S.A.*, *101*(23), 8542–8546.
Shreve, R. L. (1966), Statistical law of stream numbers, *J. Geol.*, *74*(1), 17–37.
Shroder, J. F., Jr., R. A. Scheppy, and M. P. Bishop (1999), Denudation of small alpine basins, Nanga Parbat Himalaya, Pakistan, *Arct. Antarct. Alp. Res.*, *31*(2), 121–127.
Smith, T. R., and F. P. Bretherton (1972), Stability and the conservation of mass in drainage basin evolution, *Water Resour. Res.*, *8*(6), 1506–1529, doi:10.1029/WR008i006p01506.
Snyder, N. P., K. X. Whipple, G. E. Tucker, and D. J. Merritts (2003), Importance of a stochastic distribution of floods and erosion thresholds in the bedrock river incision problem, *J. Geophys. Res.*, *108*(B2), 2117, doi:10.1029/2001JB001655.
Somme, T. O., O. J. Martinsen, and J. B. Thurmond (2009), Reconstructing morphological and depositional characteristics in subsurface sedimentary systems: An example from the Maastrichtian–Danian Ormen Lange system, More Basin, Norwegian Sea, *AAPG Bull.*, *93*(10), 1347–1377.
Stark, C. P., E. Foufoula-Georgiou, and V. Ganti (2009), A nonlocal theory of sediment buffering and bedrock channel evolution, *J. Geophys. Res.*, *114*, F01029, doi:10.1029/2008JF000981.
Stepinski, T., N. Marinova, P. McGovern, and S. Clifford (2002), Fractal analysis of drainage basins on Mars, *Geophys. Res. Lett.*, *29*(8), 1189, doi:10.1029/2002GL014666.
Stock, J., and W. E. Dietrich (2003), Valley incision by debris flows: Evidence of a topographic signature, *Water Resour. Res.*, *39*(4), 1089, doi:10.1029/2001WR001057.
Stock, J. D., and W. E. Dietrich (2006), Erosion of steepland valleys by debris flows, *Geol. Soc. Am. Bull.*, *118*(9–10), 1125–1148, doi:10.1130/B25902.1.
Straub, S. (1996), Self-organization in the rapid flow of granular material: Evidence for a major flow mechanism, *Int. J. Earth Sci.*, *85*(1), 85–91.
Tarboton, D. (1997), A new method for the determination of flow directions and upslope areas in grid digital elevation models, *Water Resour. Res.*, *33*, 309–319, doi:10.1029/96WR03137.
Tarolli, P., and G. Dalla Fontana (2009), Hillslope-to-valley transition morphology: New opportunities from high resolution DTMs, *Geomorphology*, *113*(1), 47–56.
Traer, M., G. Hilley, A. Fildani, and T. McHargue (2012), The sensitivity of turbidity currents to mass and momentum exchanges between these underflows and their surroundings, *J. Geophys. Res.*, *117*, F01009, doi:10.1029/2011JF001990.
Treiman, A. H. (2003), Geologic settings of Martian gullies: Implications for their origins, *J. Geophys. Res.*, *108*(E4), 8031, doi:10.1029/2002JE001900.
Tucker, G., and K. Whipple (2002), Topographic outcomes predicted by stream erosion models: Sensitivity analysis and intermodel comparison, *J. Geophys. Res.*, *107*(B9), 2179, doi:10.1029/2001JB000162.
Tucker, G. E., and D. N. Bradley (2010), Trouble with diffusion: Reassessing hillslope erosion laws with a particle-based model, *J. Geophys. Res.*, *115*, F00A10, doi:10.1029/2009JF001264.
Tucker, G. E., and R. L. Bras (2000), A stochastic approach to modeling the role of rainfall variability in drainage basin evolution, *Water Resour. Res.*, *36*(7), 1953–1964, doi:10.1029/2000WR900065.
Whipple, K., and G. Tucker (1999), Dynamics of the stream-power river incision model: Implications for height limits of mountain ranges, landscape response timescales, and research needs, *J. Geophys. Res.*, *104*, 17,661–17,674, doi:10.1029/1999JB900120.
Whipple, K., and G. Tucker (2002), Implications of sediment-flux-dependent river incision models for landscape evolution, *J. Geophys. Res*, *107*(B2), 2039, doi:10.1029/2000JB000044.
Willet, S. D. (2010), Erosion on a line, *Tectonophysics*, *484*(1), 168–180.
Willett, S. D., S. W. McCoy, J. T. Perron, L. Goren, and C.-Y. Chen (2014), Dynamic reorganization of river basins, *Science*, *343*(6175), 124876.
Willgoose, G., R. Bras, and I. Rodriguez-Iturbe (1991a), A coupled channel network growth and hillslope evolution model 1. Theory, *Water Resour. Res.*, *27*(7), 1671–1684, doi:10.1029/91WR00935.
Willgoose, G., R. L. Bras, and I. Rodriguez-Iturbe (1991b), A physical explanation of an observed link area-slope relationship, *Water Resour. Res.*, *27*(7), 1697–1702, doi:10.1029/91WR00937.